ISTANBUL TECHNICAL UNIVERSITY ★ GRADUATE SCHOOL OF SCIENCE ENGINEERING AND TECHNOLOGY

INVESTIGATION OF STRUCTURAL HEALTH MONITORING OF A HIGH RISE BUILDING

M.Sc. THESIS

Berkay ALDIRMAZ

Department of Civil Engineering

Structure Engineering Programme

JUNE 2020

ISTANBUL TECHNICAL UNIVERSITY ★ GRADUATE SCHOOL OF SCIENCE ENGINEERING AND TECHNOLOGY

INVESTIGATION OF STRUCTURAL HEALTH MONITORING OF A HIGH RISE BUILDING

M.Sc. THESIS

Berkay ALDIRMAZ
(501161003)

Department of Civil Engineering

Structure Engineering Programme

Thesis Advisor: Prof. Dr. Alper ILKI
Thesis Co-Advisor: Prof. Dr. Koichi KUSUNOKI

JUNE 2020

İSTANBUL TEKNİK ÜNİVERSİTESİ ★ FEN BİLİMLERİ ENSTİTÜSÜ

YÜKSEK KATLI BİR BİNANIN YAPISAL SAĞLIK İZLEMESİNİN İNCELENMESİ

YÜKSEK LİSANS TEZİ

Berkay ALDIRMAZ
(501161003)

İnşaat Mühendisliği Anabilim Dalı

Yapı Mühendisliği Programı

Tez Danışmanı: Prof. Dr. Alper İLKİ
Eş Danışman: Prof. Dr. Koichi KUSUNOKİ

HAZİRAN 2020

Berkay ALDIRMAZ, an M.Sc. student of ITU Graduate School of Science Engineering and Technology student ID 501161003, successfully defended the thesis/dissertation entitled "INVESTIGATION OF STRUCTURAL HEALTH MONITORING OF A HIGH RISE BUILDING", which he prepared after fulfilling the requirements specified in the associated legislations, before the jury whose signatures are below.

Thesis Advisor :	**Prof. Dr. Alper İLKİ** Istanbul Technical University	....
Co-advisor :	**Prof. Dr. Koichi KUSUNOKİ** University of Tokyo	....
Jury Members :	**Prof. Dr. Alper İLKİ** Istanbul Technical University	....
	Prof. Dr. Koichi KUSUNOKİ University of Tokyo	....
	Prof. Dr. Konuralp GİRGİN Istanbul Technical University	....
	Assoc. Prof. Ufuk Yazgan Istanbul Technical University	....
	Prof. Dr. Hilmi LUŞ Boğaziçi University	....

Date of Submission : 04 May 2020
Date of Defense : 05 June 2020

To my family,

FOREWORD

I would like to express deepest my gratitude to my advisor Prof. Alper Ilki and my co-advisor Prof. Kusunoki Koichi for their competent advice, endless support, recommendations, and friendships throughout my thesis study.

I would like to express my thanks to Prof. Hilmi Lus¸ for the advice, support, his time, and valuable contributions to my master thesis.

I would also like to express my gratitude to my dissertation committee members Prof. Konuralp Girgin and Assoc. Prof. Ufuk Yazgan for providing valuable insights into my thesis and their kind attitude towards me.

I would like to acknowledge Yapi Teknik and Rise Structural Engineering for providing technical support, their help, and time during my studies.

I am thankful to Prof. Masaomi Teshigawara, Prof. Akira Tasai, Prof. Yo Hibino, Prof Kenji Kabayama, and Mr. Masayuki Araki for their help, friendships, and recommendations during my field studies. Besides, I am very thankful to them for introducing me to their culture, perspective of academical and life ethics, and the way of working.

I would like to express my deepest appreciation to Assoc. Prof. Omer Tugrul Turan and Assoc. Prof. Ayse Peker Dobie for their support and for showing me the joy of intellectual pursuit.

I would like to express my sincere gratitude to my beloved friends, Mr. Berk Turkel, Mr. Asan Adamanov for the joy of living and the sincere support they have given over the years.

Finally, many gratefully special thanks to my mother Necla Aldirmaz, my father Ferhan Aldirmaz, and my sibling Hurrem Aldirmaz for their understanding, love, and support throughout my life.

June 2020

Berkay ALDIRMAZ
(Civil Engineer)

TABLE OF CONTENTS

Page

ABBREVIATIONS

ACC	: Acceleration
APSD	: Auto Power Spectral Density
CPSD	: Cross Power Spectral Density
DISP	: Displacement
DIR	: Direction
DFT	: Discrete Fourier Transform
EW	: East and West Direction
EQ	: Earthquake
FE	: Finite Element
FEM	: Finite Elements Method
FEMA	: Federal Emergency Management Agency
FT	: Fourier Transform
FFT	: Fast Fourier Transform
GPS	: Global Position System
LVDT	: Linear Variable Differential Transformer
Mw	: The moment magnitude
MDOF	: Multi-Degree-of-Freedom System
MEMS	: Micro Electro Mechanical System
NS	: North and South Direction
PSD	: Power Spectral Density
RC	: Reinforced Concrete
SDOF	: Single-Degree-of-Freedom System
SHM	: Structural Health Moınitoring
TSC	: Turkish Seismic Code
TSDC	: Turkish Seismic Design Code
TS500	: Turkish Standards for RC Structures
UD	: Up and Down Direction
VEL	: Velocity
WT	: Wavelet Transform

SYMBOLS

C40	: 40 MPa- class concrete
E	: Modulus of elasticity
f	: Frequency
F	: Floor
g	: Gravitational acceleration
Gal	: Unit of acceleration
Hz	: Hertz
km	: Kilometer
kN	: Kilonewton
m	: Meter
M	: Magnitude
min	: Minute
s	: Second
T	: Period
ξ	: Damping ratio
ω	: Angular Frequency
π	: Pi

LIST OF TABLES

Page

LIST OF FIGURES

Page

INVESTIGATION OF STRUCTURAL HEALTH MONITORING OF A HIGH RISE BUILDING

SUMMARY

High-rise buildings must be designed bearing in mind the possibility of an earthquake in earthquake-prone megacities such as Istanbul. Additionally, the health of the existing high-rise buildings must be constantly controlled before, during, and after an expected earthquake. The structural health monitoring system is used to observe the dynamic conditions of existing structures and their behavior during the earthquake. In addition to system identification techniques, structures can also be examined through their mathematical models. Therefore, the models of the existing structures need to including existing masonry infill walls and soil-structure interaction, which influence the real behavior of the structures.

The main aim of this thesis is to build a correlation between dynamic properties from on-site measurements and finite element analysis of the high-rise building by correcting the FE model of the building based on the investigation of SHM of the building. For this purpose, the study was carried out on a high-rise building in Fikirtepe, Istanbul. A system to monitor the building for twenty-four hours a day over seven days was installed. Moreover, the finite element model of the building is modeled with the package program, ETABS v16.0.0. The study was conducted on the response of the building during the earthquake that struck southwest of Istanbul in the Marmara sea, Silivri deficits, on Sept 26, 2019.

Ambient vibration records of the building are examined by the frequency domain decomposition. With the method, the natural periods and mode shapes of the building are obtained. As a result of the analysis carried out before and after the earthquake, it is found that the building has a linear behavior during the earthquake. Additionally, the response of the building during the earthquake is investigated through acceleration-time history. The transfer functions are obtained by using Fourier Transform and power spectral density method. The predominant period, model shapes, and damping ratio are calculated according to field measurements. Peak values of acceleration, velocity, and displacement time history of the building on the 16th floor are determined during the earthquake. Fourier Transform and Wavelet Transform methods are used to find these values. The results of the experimental test are compared with the analysis results of the package program, SeismoSignal.

In addition to the experimental study, the mathematical model of the building is created. The building is modeled based on the design phase. When the dynamic properties of the model are defined, it is observed that it does not match the field test results accurately. The finite element model which correlates the identified modal results of the building is developed. Infill walls and soil-structure interaction, which are ignored during the design phase of the building, are included in the model. The earthquake input motion taken from field measurement is performed for the building by linear time history analyses. The results are compared with the results of the in-situ measurement. It is observed that the corrected finite element model better represents

the behavior of the existing building than the design values in the linear stage. In this study, it is shown that modeling the structure with real parameters such as infill walls and soil-structure interaction is significant in the determination of the model dynamics and the behavior of the structure during the earthquakes.

YÜKSEK KATLI BİR BİNANIN YAPISAL SAĞLIK İZLEMESİNİN İNCELENMESİ

ÖZET

Yüksek binalar, İstanbul gibi deprem eğilimli mega şehirlerde deprem olasılığı göz önünde bulundurularak tasarlanmalıdır. Aynı zamanda inşası tamamlanmış yapıların sağlığının sürekli olarak kontrol edilmesi gerekmektedir. Yapı sağlığı izleme sistemleri var olan yapıların mecvut güvenlik durumlarını ve olası bir deprem sırasındaki davranışını gözlemlemek için kullanılır. Sistem tanılama yöntemlerinin yanı sıra, yapı matematiksel modeli aracılığı ile de incelenebilir. Bunu takriben mevcut yapıların davranışını etkilen dolgu duvarlar ve yapı zemin etkileşiminin matemetiksel modele yansıtılması gerekmektedir.

Bu tez çalışmasının temel amacı, yerinde alınan kayıtlar aracılığı ile bulunan yüksek katlı yapının dinamik özellikleri ile bu yapının sonlu elemanlar analizi arasında bir korelasyon oluşturmaktır. Bu amaç doğrultusunda İstanbul Fikirtepe'de bulunan çok katlı bir bina üzerinde çalışmalar yapılmıştır. Bu binanın yedi gün yirmi dört saat izlenmesini sağlayacak bir sistem binaya yerleştirilmiştir. Ayrıca bu binanın sonlu elemanlar modeli, paket program yardımıyla oluşturulmuştur. Çalışma, 26 Eylül 2019 tarihinde Mw=5.8 olan ve Silivri açıklarında gerçekleşen depremin bu bina üzerindeki etkileri üzerinden sürdürülmüştür.

Yapının çevresel titreşim kayıtları frekans tanım aralığında ayrıştırma tekniği ile incelenmiştir. Bu metot ile yapının doğal periyotları ve mod şekilleri bulunmuştur. Deprem öncesi ve sonrası alınan kayıtlar incelenmiştir. Yapılan analizler sonucunda, yapının deprem sürecince doğrusal davranış sergilediği bulunmuştur. Ek olarak, binanın depreme verdiği tepki sadece ivme kaydı aracılığı ile incelenmiştir. Fourier Transformu ve güç spektral yoğunluğu metotları kullanılarak transfer fonksiyonları oluşturulmuştur. Yapının baskın periyodu ve sönüm oranları hesaplanmıştır. Deprem süresince, yapının en üst katındaki ivme, hız ve yer değiştirme tepe değerleri bulunmuştur. Bu değerleri bulabilmek için Fourier ve Wavelet Transformu metotları kullanılmıştır. Yapılan analizlerin sonuçları, paket program olan SeismoSignal analiz sonuçları ile kıyaslanmıştır.

Numerik çalışmanın yanı sıra, yapının matematiksel modeli de oluşturulmuştur. Tasarım aşaması temellerine dayanarak yapı modellenmiştir. Bu modelin dinamik karakterizasyonu yapıldığında nümerik sonuçlarla örtüşmediği görülmüştür. Yapının, nümerik analiz sonuçlarını yansıtabilecek analitik modelin kurulabilmesi için sonlu elemanlar modeli düzeltilmiştir. Yapının tasarım aşamasında göz ardı edilen dolgu duvarlar ve yapı-zemin etkileşimi modele dahil edilmiştir. Güncellenmiş sonlu eleman modeli üzerine Marmara depreminde zemin seviyesindeki ivmeölçerden alınan ivme-zaman kaydı uygulanmıştır. Yapının doğrusal zaman tanım aralığında analizi yapılmıştır. Analiz sonuçları, sahada ölçülen sonuçlarla karşılaştırılmıştır. Düzeltilmiş sonlu elemanlar modelinin yapının gerçek davranışını daha iyi yansıttığı görülmüştür.

1. INTRODUCTION

1.1 Overview

The growing world population's demand for housing also grows constantly. High-rise buildings are a solution to this demand in megacities with limited land available for construction. High-rise buildings address the need for more accommodation at lower cost within a limited area. Additionally, they are high prestige properties due to their high-tech design and construction. On the other hand, more caution is needed for the construction of high rise buildings since they can be more hazardous than the simple buildings during seismic events. These risks may cause with huge economic losses and, even worse, the loss of large number of human lives. Therefore, the complexity and uncertainties of high rise buildings have to be investigated more deeply. The effects of the soil-structure interaction along the basement floor located under the ground level and the infill walls used in the existing buildings can be pointed out as the two major uncertainties of the high rise buildings. In addition, the health of the high rise buildings has to be monitored and evaluated before, during, and after seismic events.

In recent years, structural health monitoring systems have been used for many existing structures to gather information about their dynamic characteristics and current conditions. With the rapid developments in technologies, it is easier to install data acquisition systems to the structures. The dynamic parameters and behaviors of the structures can be determined realistically by examining the response records taken from the existing structures located in earthquake-prone areas. According to previous studies conducted by researchers, definitions of structural health monitoring are described below:

Housner et al. (1997) define structural health monitoring. Structural health monitoring aims to identify the alterations which may specify damage or deterioration by calculating the behavior of the structure and nondestructive detection on the field [1].

Worden et al. (2007) identify that structural health monitoring refers to the operation of executing a damage detection strategy to use in the areas of aerospace, civil, and mechanical engineering [2].

Catbas et al. (2000) explain that health monitoring, which constitutes the foundation of an integrated asset management plan regarding system level for the structures, has the same path with human health management [3].

Abdo (2014) propounds that the nervous system of humans and health monitoring have a resemblance in general aspects, which is a similar approach to Catbas's view of SHM and human health management. Also, human has the nervous system which composes of the complicated network of nerves and cells that carry signals to and from the brain and the parts of the whole body. Every part of the human body is linked with the brain via the nervous system because the brain which receives and analysis the signals transmitted from the body has the authority of implementation of the instructions. The nervous system is analogous to structural health monitoring which is composed of a sensory system and control unit. The sensory network is used to gather information whereas the control unit is used for data processing and decision making [4].

Wide abroad view of the concept of structural health monitoring are organized below:

- Building instrumentation,
- Gathering data and transmission system,
- Digital signal processing, and
- Implementation of the evaluation technique to the structural system.

Structural health monitoring aims to monitor the response of the structures and identify the damage by analyzing data taken from in-situ measured data. This data is highly open to deteriorate due to field conditions and sensitivity of data, therefore, selecting the equipment which is used for monitoring the structure requires to be cautious. To gather data, the instrumentation plan of the building and sensory system has a critical role in the monitoring structure. Using correct sensors are extremely significant to collect data accurately regarding your purpose. Also, equipment properties are needed to be accurate sensitivity to evaluate the behavior of the structure by the structural health monitoring system. GPS displacement, acceleration, strains, wind velocity detectors, linear variable differential transformers (LVDT), etc. can be used as monitoring equipment. The use of the items alters depending on the aim of the project. Some of the sensors and equipment that can be used for monitoring are listed up in Table 1.

Table 1.1 : Sensors and Equipment list

Sensors and equipment	Purpose
Accelerometer	Vibration (Ground, Structure, etc.)
LVDT	Displacement
Global Position System (GPS)	Displacement
Anemometer	Wind speed
Strain transducer	Strain
Tiltmeter	Displacement

1.2 Significance, Objectives, and Scope

Istanbul is a growing metropolis in a seismically active zone with diminishing construction areas. In recent years, many high rise buildings have been constructed in the city which, is in a high-risk earthquake zone, without sufficient consideration of the influence of infill walls and soil-structure interaction. In this study, a high-rise building in Istanbul was instrumented with accelerometers to create a more accurate FE model based on the SHM of the building. System identification of the building was carried out via OMA techniques. Moreover, the FE model of the building is step by step corrected by adding infill walls and soil-structure interaction to the model. The response of the building recorded during an M5.8 earthquake is determined by both FE and SHM techniques. The results of both in-situ measurements and each FE model are compared. The study shows that adding the parameters, which influence the existing building, to the FE model of the building has a crucial role to reflect the real behavior of the building according to SHM results. The path followed during the study is demonstrated in Figure 1.1.

This work consists of 5 sections. This study is organized according to each step of procedures as follows:

Section (1) introduces the significance, objectives, and scope of the dissertation. Also, the SHM systems, the effect of masonry infill walls on the structure, soil-structure interaction, and recent technologies that are developed by the researcher are summarized.

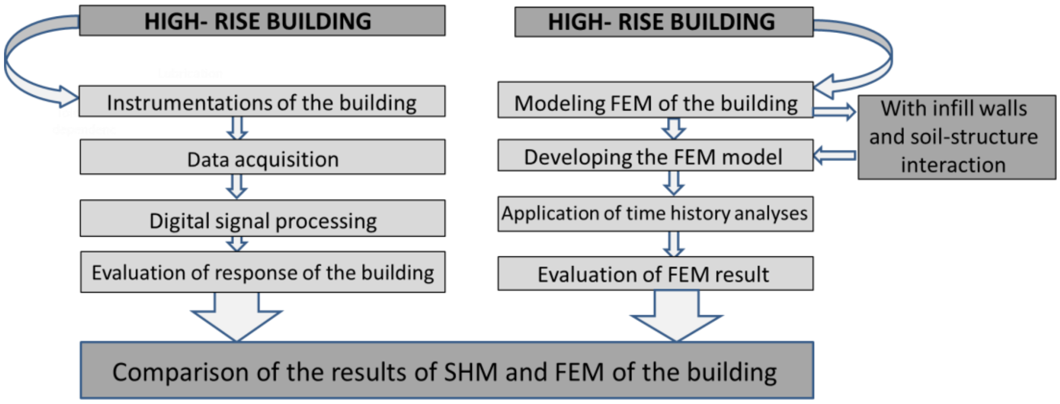

Figure 1.1 : Draft paths of the thesis

Section (2) introduces the instrumentation of the existing building. In addition, digital signal processing is introduced briefly. It should be noted that no attempt has been made to a deep understanding of every detail of the structural health modeling technique. The chapter covers the results of system identification. The outcomes obtained from in-situ measurements are integrated into velocity and displacement. The results of the experimental study are also represented.

In section (3), the finite element model is corrected in detail. The structural system and the location of the building are described. Moreover, different modeling techniques are discussed in the direction of including existing parameters to the model of the building. Procedures for correcting the finite element model of the building are explained. Results that are obtained from the mathematical models are shown.

Section (4) compares the analyses results taken from a finite element model and structural health monitoring of the building. Moreover, the comparison of the results system identification and mathematical models of the high-rise building is also indicated. Response displacement of the earthquake input is presented.

In section (5), conclusions and recommendation following the summary of the study are represented, The findings of the dissertation are discussed.

The plan of the thesis is as follows: the some of the structural health monitoring techniques and the results of the on-site measurements are represented in section (2), procedures of correcting the finite element model of buildings and their analyses results are shown in sections (3), the comparison of the results are discussed in section (4), and the conclusion and recommendations are given in section (5).

1.3 Summary of Previous Applications

Kusunoki and Teshigawara (2004) attempt to enhance a new judgement system that makes calculations automatically using a few inexpensive accelerometers. The purpose of developing a new examination system is to decrease the number of people who run away from their house and extra damage to structures because of aftershocks. The developed system is enabled to specify the safety level of a building. The spectrum method is used in order to judge the buildings. The proposed judgement, a new real-time residual seismic capacity evaluation system, is based on the prediction of residual seismic capacity of the structure by comparing performance and demand curves. The performance curve can be drawn according to the absolute response accelerations and the relative response displacement. Thus, a double integral technique that is applied to measured acceleration to derive the response displacement is discussed. The accuracy of this proposed system is checked with the shaking table test results of steel frame structures. 3 specimens which are one span plane steel frame structure is tested. Columns and beams are steel plats. The width and thickness of the plats are 100 mm and 6 mm, respectively. 1-story, 2-story, and 3-story specimens are used. The height of the first story is 595 mm, the second and third stories are 600 mm. The length of the span is 1,000 mm. Masses that have 190 N weight are placed to the nodal points of the steel frame structure. For the input motion, the steel frame is exposed to the NS component of the El Centro earthquake record. Transducers that are located in each story are used to confirm the validity of the integration method and the performance curve. It is seen that the integration method is needed to improve to get more accurate displacement. Also, the authors conclude that residual seismic capacity evaluation can calculate by the prosed system [5].

Kusunoki, Elgamal, Teshigawara, and Conte (2008) apply the wavelet transform method to dynamic response data gathered from Vincent Thomas Bridge which is suffered from the Whittier earthquake (1987) and Northridge earthquake (1994). The Vincent Thomas Bridge is a steel bridge that is a cable-suspension. The total length of the bridge is 1850 m with a center span of 720 m, each side of the suspended span of 154 m, and 545 m long on each end. 26 accelerometers were placed on the bridge in 1980. Data are sampled at 50 Hz. One of the major reasons why the bridge was used is that not only predominant mode but also other modes affect the response due to the length of the bridge. The wavelet transform which decomposes a signal in the temporal domain method is primarily applied to the measured acceleration in order to reach an accurate performance curve. The researches indicate that the predominant performance curves of the bridge can be extracted using the wavelet transform method, successfully [6].

Kusunoki, Tasai, and Teshigawara (2012) discuss the performance curve, stiffness degradation, observed crack patterns, and the histories of predominant periods and stiffness since 2009 according to the proposed evaluation technique which is applied to Yokohama National University. The key point on the proposed evaluation method is the deriving response displacement from actual accelerations. Double integral is applied by the wavelet transform method. The height of the 9-story (8-story and 1 underground floor) reinforced concrete building is 30.8 m. The building was instrumented in 2008 and the data has been recorded since then 2008. During 2011 Off the pacific Tohoku earthquake is also measured by accelerometers very well. The monitoring system records the maximum acceleration of 91.5 cm/s^2 in the basement and 410 cm/s^2 on the roof. Multi-degree-of-freedom system (MDOF) is converted to the single-degree-of-freedom system (SDOF) to simplify the restoring force and deformation of representative displacement for analyzing the nonlinear response. According to the result of the analysis of the proposed method, the building is still able to carry more lateral forces; plus, stiffness decreases because of cracking, not because of yielding. In addition, since the building is exposed to damage during 2011 Off the Pacific Coast of Tohoku Earthquake, the periods become longer in both directions. Finally, due to cracks which are occurred during the earthquake, the degradation of the performance curve is calculated accurately. Also, the record allows deriving the relationship between story shear force and inter-story drift [7].

Kusunoki (2016) proceeds progress on residual seismic capacity evaluation system by applying his study to the base-isolated building. The Earthquake Research Institute of Tokyo University which is a three-building, base-isolated complex, was selected as a target building. Instrumentations were placed to the target in 2006 and recorded the dynamic response of the building during the Tohoku Earthquake very well. Since the measured acceleration effects from the error components, the wavelet transform is used to eliminate the error components of the acceleration. Then, the capacity spectrum method is applied to the nonlinear response of building which is a multi-degree-of-freedom system, in order to simplify to the single-degree-of-freedom system. Through this study, Kusunoki shows that the capacity spectrum method works properly to estimate the maximum response of the building and the wavelet transform technique is highly efficient to derive the displacement from the acceleration [8].

On the other hand, the dynamic properties of the building can be examined only through ambient vibrations, besides evaluating the behavior of the buildings under earthquake. Since ambient vibrations cannot be measured independently of the structure, the data contain information about the response of the building. By using modal analysis methods, it is possible to obtain information about the dynamic characteristic and behavior of the system through on-site ambient vibration testing and compare them with design values. Studies have shown that field measurement values and design values do not overlap. The difference between these values has high significance, especially for high-rise buildings. Many tests in the literature have been conducted to investigate the effects of masonry infill walls on the character of the high rise buildings.

Zhou et al. examined the dynamic behavior of 10 high rise buildings in Laibin. Modal analyses were executed on ambient vibrations for this investigation. The natural periods and mode shapes of the structures were calculated via operational modal analyses. Besides, analytical models were created to determine the dynamic properties of the high rise buildings. Six different finite element models were modeled to discuss the influences of the infill wall mass and stiffness on the dynamic characterizations of the buildings. Analytical and experimental results were compared to make a correlation between the dynamic properties of the buildings. Furthermore, the proposed 25 empirical equations in the literature were used to predict fundamental periods of 10 high-rise buildings. It has been shown that the predominant periods of the buildings are higher than the measured fundamental periods when either stiffness or mass of infill walls are ignored in mathematical modeling. Consequently, the importance of modeling infill walls in mathematical models is stated [9].

Mohammed et al. were studied on an 18-floor building to observe the effects of infill walls. The building was damaged during the Gorkha Earthquake that occurred in 2015 with M7.8. The system identification and finite element modeling were examined. Fifteen accelerometers at different setups and three seismometers were set up to measure the ambient vibration. The modal identification results obtained from the two monitoring systems were compared. Besides, two different finite element modelings were created to investigate the influence of the infill walls. Reduced factors were used to express stiffness of the damaged infill walls. The developed mathematical model considering the non-structural elements reasonably matched with the natural periods of the building obtained from system identification [10].

2. STRUCTURAL HEALTH MONITORING (FEM) OF THE BUILDING

Every particle has its movement which is called vibration. Vibration gives information about the behavior of particles if it can be analyzed accurately. If the general system is considered, rather than the particles, the methodology does not change, which means that the behavior of a structural system can be estimated by analyzing vibration data taken from the system. Fundamental of structural health monitoring is based on vibration and processing the vibration.

Constant dead loads, live loads, alterations of environmental conditions, and environmental events such as an earthquake affect the conditions of all structures adversely. As a consequence of these effects, damages occur on structures with time. Thus, instead of routine control or critical-event based inspections such as an earthquake, monitoring structures enable to estimate of the evaluation of structural conditions using real-time data. Regarding this need, structural health monitoring is a rising trend subject to structural engineering [5].

2.1 Instrumentation of The Building

The tall building was designed as reinforced concrete (RC) building according to the Turkish Seismic Code (TSC) (2007) in 2015. After completing the design of the building, the construction of the building was finalized in 2018. The building which is located in Fikirtepe, Kadıköy, Istanbul (Figure 2.1) was instrumented in 2019. Since 2019, the building has been monitoring continuously. The building is a part of a complex with three towers. In addition to seven basement floors which are used as parking areas, all towers have shopping areas on the ground floor. On this project, the investigation is carried out only one of the towers which are marked with a red circle in Figure 2.2. Furthermore, the building has 25 stories and 7 of which are below the ground level. The reinforced concrete system consists of slabs, beams, columns, and shear walls. The building has a mat foundation having a sectional depth of 150 cm. The soil consists of rock components. Modulus of horizontal subgrade reaction and allowable soil stress is 1,200,000 kN/m^3 and 700 kN/m^2, respectively.

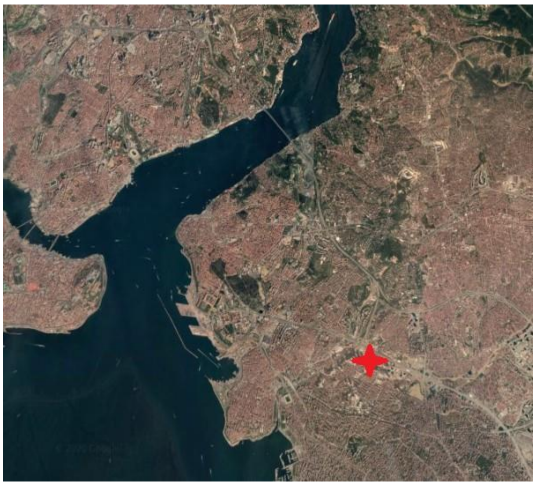

Figure 2.1 : Location of the building with respect to the Bosphorus.

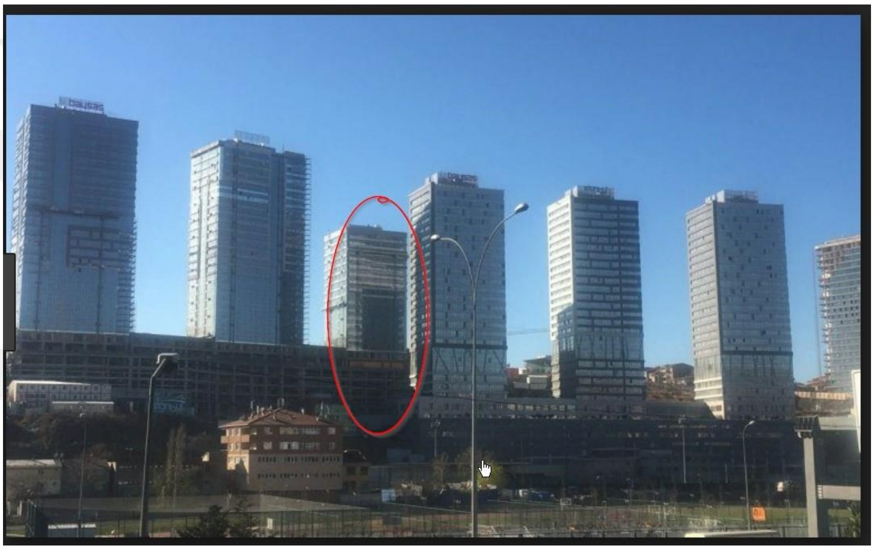

Figure 2.2 : The instrumented building in the complex.

Before the instrumentation, defining the possible location of the sensors is crucial to monitor the building accurately. In high-rise buildings, it is significant to have sufficient torsional stiffness around the vertical axis as well as bending stiffness in two directions. In the arrangement of suitable stiffness, the first two periods of vibrations are expected to be bending in two directions, and the third of which torsional vibration. Only one accelerometer cannot be enough to set up on a floor when faced with a torsional response.

Considering these conditions, the floors may require more than one accelerometer. Moreover, the torsional behavior of the building is ignored. Thus, for each floor, the SHM system requires one sensor that is needed for the -7th floor, top, and an additional one per 3 to 5 floors. Also, the core of the building which is rounded by shear walls is selected to locate the sensors in order to record absolute response vibration of the building accurately.

Overall, the server, the receiver, the sensors, and the cables create the monitoring system. The server which is connected to the receiver on the same floor is located on the 16th floor. Totally six accelerometers which are shown in Figure 2.3 are placed to the -7th, -5th, ground, 7th, 12th, and 16th floors. All sensors and the receiver are connected via cables. The cables are arranged through the ventilation shaft shown in Figure 2.6. The receiver and the sensor placed on the 16th floor can be seen on the key plan as Figure 2.4. Additionally, ground levels of the building can be seen based on cross-sections shown in Figure 2.4 and Figure 2.5. The receiver and the 16th floor sensor are shown in Figure 2.6. In Figure 2.6, the red box, green box, and the red computer represent the location of accelerometer, receivers, and server, respectively.

Figure 2.3 : The locations of the sensors on the floors.

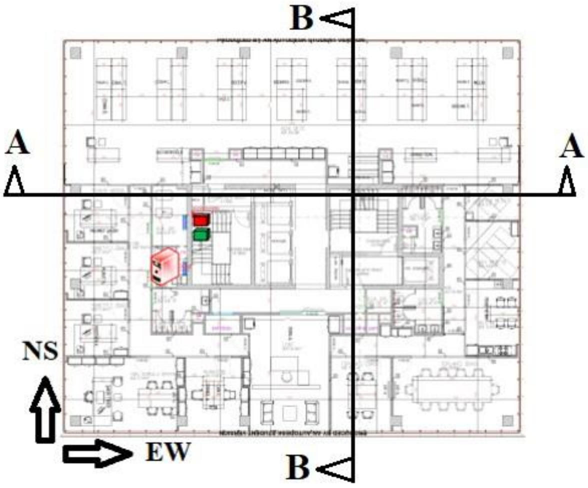

Figure 2.4 : The location of the sensor, receivers, and server on the key plan.

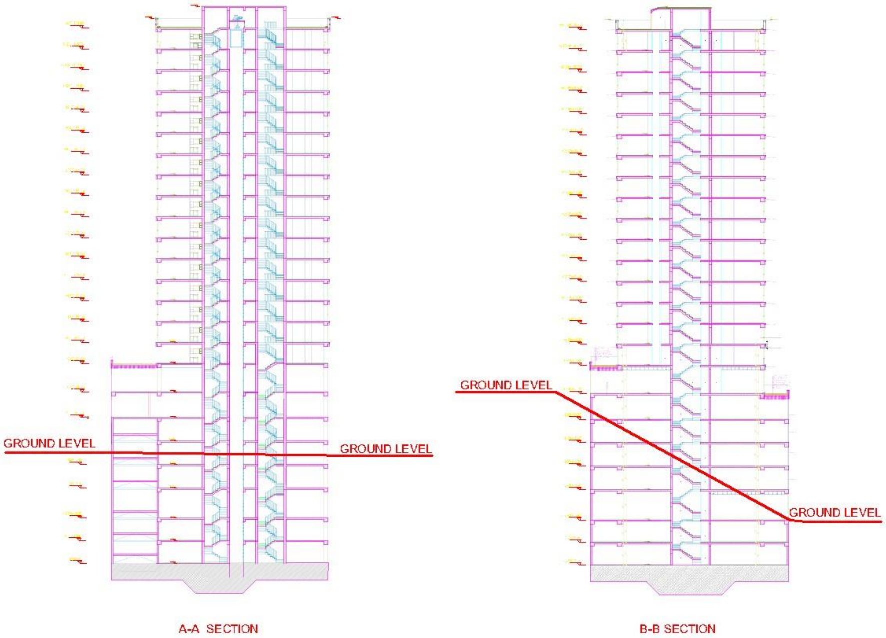

Figure 2.5 : The ground levels of the building.

Figure 2.6 : Ventilation shaft and located receiver and the sensor on the 16th floor.

Two of PoE Hub Switches with 5 ports which supply power over ethernet are used as a receiver. It allows power, communication, and time synchronization using only a single cable. Therefore, sensors do not need to plug into any other power supply additionally. While PoE technology reduces cabling and installation time, it also optimizes communication. Furthermore, three types of accelerometers are used during the study. The first one, IoLAM-02, is used for 6 indicated floors. However, the accelerometers located between -7th and 16th floors are replaced with the second type of ADXL355 due to technical problems after Sep in 2019. Until the change, ambient vibration of the building could not be recorded on the apart from -7th and 16th floors. The last type of SENSEBOX703X was used just for one day ambient vibration record on the date of October 28, 2019. This sensors were located at -5F, -1F, 7F, 12F, and 16F. These devices are micromechanical system (MEMS) acceleration sensors which use a pendulum. Specifications of the accelerometers are shown in the following Table 2.1.

Table 2.1 : Presents the details of the accelerometer specifications

	Acceleration Type		
	IoLAM-02	ADXL355	SENSEBOX703X
Measurement	Triaxial	Triaxial	Triaxial
Measurement range	±2.5G	±3.0G	±1.0G
Sampling rate	100 Hz	100 Hz	100 Hz
Noise density	25μg/√Hz	20μg/√Hz	70μg/√Hz

All sensors have their local IP which links to global IP into the server. It allows reaching the system using the internet. This makes it available for the users to control the system via website remotely. Moreover, after setting a threshold value, recording data automatically is possible when the acceleration values are higher than that thresholds. This provides an event-driven option such as possible earthquakes or wind events to be accessible. In addition, monitoring the building for 7 days and 24 hours is available. The general working principle of the monitoring system is demonstrated in Figure 2.7.

The system that is installed the building are capable of:

- recording raw data,

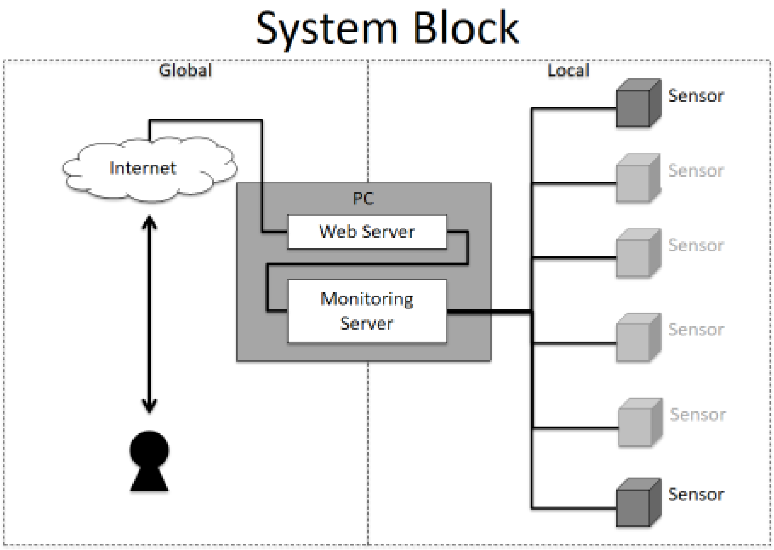

Figure 2.7 : Working principle of system block.

- summarizing peak records,
- calculating Fast Fourier Spectrum and transfer function of an event, and
- determining the capacity curve of all ranks of events using the Wavelet Transform method.

2.2 Digital Signal Processing

2.2.1 Fourier analysis method

Signals which are composed of series of periodic functions can be decomposed as a sinusoidal and cosinusoidal function by scaling amplitudes and frequencies. Furthermore, signals in the time domain can be expanded by the following Fourier series.

$$x(t) = \frac{a_0}{2} + \sum_{n=1}^{\infty} \left(a_n \cos\left(\frac{2\pi nt}{T}\right) + b_n \sin\left(\frac{2\pi nt}{T}\right)\right) \quad (2.1)$$

Here, T and t represent the period and time, respectively whereas the coefficients a_0, a_n, and b_n are defined by the following equations;

$$a_0 = \left(\frac{2}{T}\right) + \int_0^T x(t)dt \quad (2.2)$$

$$a_n = \left(\frac{2}{T}\right) \int_0^T x(t) \cos\left(\frac{2\pi nt}{T}\right) dt \quad (2.3)$$

$$b_n = \left(\frac{2}{T}\right)\int_0^T x(t)\sin\left(\frac{2\pi nt}{T}\right)dt \tag{2.4}$$

Signals obtained from the response of the structure have a finite duration and discrete-time. As a result, a discrete Fourier transform (DFT) is used by taking into consideration the properties of the data. Besides, the DFT is commonly used for computational purposes since it can be calculated easily by the use of the FFT (fast Fourier transform) which has a fast algorithm.

The signal consisting of N number of steps is analyzed by the following discrete Fourier series;

$$x(t_k) = \frac{a_0}{2} + \sum_{n=1}^{N/2}\left(a_n\cos\left(\frac{2\pi nk}{N}\right) + b_n\sin\left(\frac{2\pi nk}{N}\right)\right) \tag{2.5}$$

where the coefficients a_0, a_n, and b_n are given by the following equations, respectively.

$$a_0 = \left(\frac{2}{n}\right)\sum_{k=1}^{N} X_k \tag{2.6}$$

$$a_n = \left(\frac{1}{n}\right)\sum_{k=1}^{N} X_k cos\left(\frac{2\pi nk}{K}\right) \tag{2.7}$$

$$b_n = \left(\frac{1}{n}\right)\sum_{k=1}^{N} X_k sin\left(\frac{2\pi nk}{K}\right) \tag{2.8}$$

2.2.2 Auto- and cross- power spectral density

Power spectral density (PSD) of a signal shows the intensity of the alteration in the signal as a frequency function. The Power Spectral Density (PSD) is defined as the Fourier Transform (FT) of the auto-correlation function. The purpose of estimating spectral density is to detect any periodicity in the signal by observing peaks at frequencies corresponding to these periodicities.

The cross power spectral density (CPSD) describes the relationship of two signals regarding power distribution in the frequency domain. CPSD can identify the frequency response of the structure from its ambient vibration record which has low amplitude and noise. While determining the cross-correlation of the signals, the method takes into account the amplitude and phase response of the system. The ambient vibration of the structure consists of the input data and the response of the structure. The input data does not have the predominant frequencies; thus, applying the method to the response data of the structure allows to reflect the behavior of the system directly.

CPSD of a pair of recorded data with finite duration can be determined by the Wiener-Khintchine relation as a Fourier transform of the cross-correlation function and the signals shown in the following equations [11];

$$S_{xy}(f) = \int_{-\infty}^{\infty} S_{xy}(\tau) e^{-j2\pi f\tau} d\tau \tag{2.9}$$

$$X_k(f,T) = \int_0^T x_k(\tau) e^{-i2\pi f\tau} d\tau \tag{2.10}$$

$$Y_k(f,T) = \int_0^T y_k(\tau) e^{-i2\pi f\tau} d\tau \tag{2.11}$$

where S_{xy} represents the Fourier transform of the cross-correlation function, R_{xy} is cross-correlation function, and X_k and Y_k are the Fourier transform of the signals $X_k(t)$ and $Y_k(t)$ are the signals, respectively. The following equations represent auto- and cross-spectral density functions.

$$S_{xx}(f) = \lim_{T\to\infty} E\left[\frac{1}{T} X_k^*(f,T)\, X_k(f,T)\right] \tag{2.12}$$

$$S_{yy}(f) = \lim_{T\to\infty} E\left[\frac{1}{T} Y_k^*(f,T)\, Y_k(f,T)\right] \tag{2.13}$$

$$S_{xy}(f) = \lim_{T\to\infty} E\left[\frac{1}{T} X_k^*(f,T)\, Y_k(f,T)\right] \tag{2.14}$$

Where * represents the complex conjugate of the signal.

To estimate the auto- and cross- power spectral density, csd Matlab code which uses Welch's averaged periodogram method is used. The code is changed with cpsd code with subsequent updates of Matlab but it is still available for the same usage. DFT length, sampling frequency, windowing function, and an averaging number are needed to apply this code as shown below;

Pxy = csd(x,y,WR,SF,window(WS),a_num)

Pxx = csd(x,x,WR,SF,window(WS),a_num)

where Pxy and Pxx represent the cross- and auto- power spectral density respectively, x and y represent the collected data from sensors, WR represents the number of DFT points, SF represents sampling frequency, window(WS) represents window function with sampling frequency, and a_num represents an averaging number.

This code is run with a resolution of 2048 points, 100 HZ sampling frequency, a Hanning window filter, and an averaging number with the Matlab default value.

2.2.3 Transfer function

In general, the transfer function is used to define the correlation between the input and output which are considered in this work as a measured response acceleration taken from the accelerometer of 16F and -7F, respectively. If the Fourier transform of the input and output exists, then the transfer function can be expressed as below.

$$H = \frac{FFT\ of\ output}{FFT\ of\ input}$$

Besides, the transfer function can be described in terms of the power spectral density shown in the following formula. Figure 2.8 shows the basic idea of the transfer function.

$$h(t) = \frac{S_{xy}(f)}{S_{xx}(f)}$$

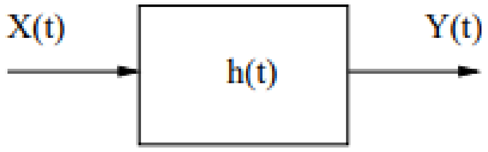

Figure 2.8 : Relationship between input, X(t), output, Y(t), and transfer function, h(t).

The Fourier transform identifies the dominant frequency of the signal with its magnitudes. However, the signal obtained from the measured acceleration of the response of the structure contains not only dominant frequency but also some other dynamic characterization of the structure such as damping ratio. Therefore, the validity of the transfer function obtained from FFT is examined by fitting the theoretical expression of the following transfer function;

$$F(x)i = \left\{ \left| \sum_{S=1}^{N} {}_S u_i \, {}_S \beta \sqrt{\frac{1 + 4_S h^2 \left(\frac{X}{F_S}\right)^2}{\left[1 - \left(\frac{X}{F_n}\right)^2\right]^2 + 4_S h^2 \left(\frac{X}{F_S}\right)^2}} \right|_i \right\} \tag{2.15}$$

where F_S, X, h, and ${}_u\beta$ represent predominant frequency, frequency of output, damping ratio, and participating factor, respectively.

In addition, the transfer function obtained by FFT may have more than one peak for one dominant frequency. However, in this case, it is not easy to estimate the predominant frequency corresponding to this interval in consideration. Thus, fitting the theoretical transfer function to the transfer function may be used in order to find the predominant frequency.

2.2.4 Wavelet transform

The Fourier expansion can be expressed as a sum of a series of sines and cosines. Therefore, the Fourier theory is able to determine all the frequencies presence in a stationary signal or function with high-frequency resolution.

The reason why non-stationary signals are not suitable for Fourier transformation is the structure of the continuous signal. In the Fourier transform of a continuous signal, all the frequencies in the signal can be seen hence the frequency resolution is perfect, but there is no time resolution. In other words, the transform does not indicate a certain time of these frequencies. The reason for the absence of such a problem in stationary signals is that the frequencies do not change over time.

Moreover, frequency and time resolution cannot be increased (or decreased) at the same time. When the former increases, time resolution decreases. When the latter increases, the frequency resolution decreases. This phenomenon is called Heisenberg's uncertainty principle.

On the other hand, the data obtained from the response of the structure contains a non-stationary random signal. Thus, time information is needed to specify all frequency components in the signal. One of the methods developed to overcome this issue is the Wavelet Transform (WT).

The wavelet transform is recently used to solve the shortcoming of windowing and signal- cutting. Instead of cutting the signal, the Wavelet transform uses a wavelet as a window which is shifted along to the signal and fully scalable [12]. Thus, it can work with multiple resolutions. When the system has high frequency, the window provides high time resolution but a low-frequency resolution by arranging the thickness of the wavelet. On the contrary, when the system has a low frequency, the window provides low time resolution but a high frequency resolution by applying the same procedure.

The following two fundamental differences between FT and WT are listed:

- While the FT does not calculate the negative frequencies which remain at the bottom of the window, the WT takes into consideration the negative components of the signal due to the structure of the window.

- Even though the FT has a fixed width window, the WT uses a fully scalable window through the signal.

The window which has a critical importance for the WT is called as a mother wavelet. Whether a function can be a mother wavelet depends on the following two conditions. Also, mathematical expressions of these conditions shown in equation 2.16 and equation 2.17.

- Duration of the wavelet is limited.

- The average value of the wavelet function is zero.

Due to these two conditions, the mother wavelet function should oscillate in the positive and negative aspects of the amplitude axis. Also, when this oscillation ends, the amplitude is 0 as it progresses along the time axis. This feature can be seen in Figure 2.9 for some main wavelet functions used in the WT.

$$\int_{-\infty}^{\infty} \psi\,(x)dx = 0 \tag{2.16}$$

$$\int_{-\infty}^{\infty} \psi^2\,(x)dx = 1 \tag{2.17}$$

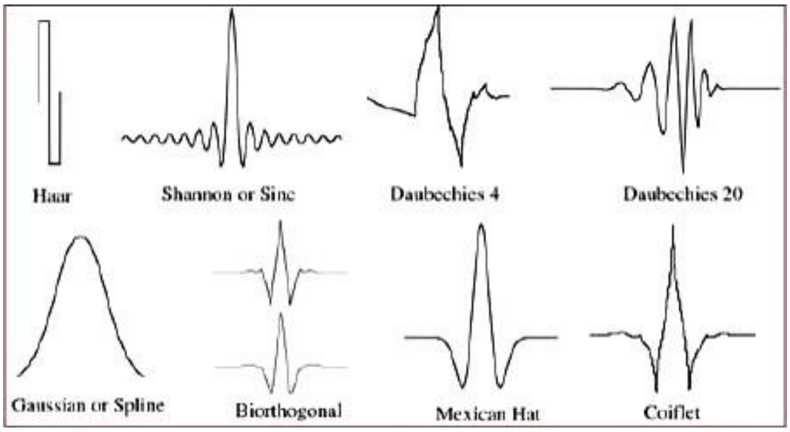

Figure 2.9 : Examples for some main mother wavelets

The WTM is a time-frequency analysis method to represent time and frequency information of the signal simultaneously by using a mother wavelet. The following steps represent the methodology of WTM [7].

The signal with N data points is decomposed into a signal with a certain frequency band, g_1, and a remainder f_1, each of which has N/2 data points shown in equation 2.18. By applying this procedure n times, one can express the original signal f_0 by following equations;

$$f_0 = g_1 + f_1 \tag{2.18}$$

$$f_0 = g_1 + g_2 + g_3 + \cdots + f_n \tag{2.19}$$

where $n = log_2 N$ and $g_1, g_2, \ldots,$ and g_n are orthogonal.

Each frequency band and the related remainder are given by the following equations;

$$g_j = \sum_k d_k{}^{(j)} \psi(2^j x - k) \tag{2.20}$$

$$f_j = \sum_k c_k{}^{(j)} \varphi(2^j x - k) \tag{2.21}$$

where ψ is the mother wavelet and φ is the scaling function.

2.2.5 Frequency domain identification

Brincker et al. developed a technique, which focuses on a frequency domain decomposition (FDD). The technique is able to identify modal parameters using output-only data. The FDD technique attempts to decompose each harmonic component in the response signal. Power spectral density (PSD) matrices of outputs are obtained corresponding to a single degree of freedom (SDOF) system by applying a Discrete Fourier Transform. Next, the singular value decomposition (SVD) of the spectral matrix is taken at discrete frequencies that give the spectral value and the mode shape of the system. SVD of the matrix can be obtained by equation 2.22 [13].

$$G_{yy}(\omega) = U(\omega) S(\omega) U^H(\omega) \tag{2.22}$$

Where $U(\omega)$ is a unitary matrix of the singular vectors and $S(\omega)$ is a diagonal matrix of singular values, and H indicates the complex conjugate and transpose.

The response of the system in the frequency domain at discrete frequency is denoted by spectral values. The first singular vector strongly estimates the mode shape and first dominant frequency of the predominant mode. Modal frequencies and mode shapes of even higher modes can be calculated by applying more precise frequency discretization to data.

2.3 Analyses of the Building

The records of before, after, and during the Marmara earthquake were examined. The dynamic properties of the building and the absolute acceleration, velocity, and displacement values on the 16th floor were obtained with the records taken by accelerometer during the earthquake. The modal frequencies of the building were found with the FDD analysis of ambient vibrations which are recorded before and after the earthquake. The other methods were also used analyses carried out to data recorded during the earthquake. The vibration response of UD direction is ignored on the thesis.

2.3.1 Ambient vibration before the earthquake

Ambient vibration of the building is recorded 6 days before the Marmara earthquake on the 20th of September in 2019. In the day time, it is highly possible to see many frequencies on the collected data due to the effects of occupant movements, maintenance of some mechanical equipment, usage of the parking area, the elevators, the heating, the air conditions, etc. On the other hand, the data is required to have minimum noise to analyze the ambient vibration accurately. Therefore, the 20 minutes data of the ambient vibration which is recorded in the early morning at 01:20 am is used.

Representative ambient vibration data taken from the -7th and 16th floor of the building can be seen in Figure 2.10 and Figure 2.11, respectively. FDD method is applied to selected data to obtain the first natural frequency of the building. Figure 2.12 represents the result of the analyses of the FDD method for ambient vibration. The structural predominant modal frequencies in EW and NS directions are shown in Figure 2.12. The first predominant period of the building in EW direction is 0.89 s while it is 1.03 s for NS direction.

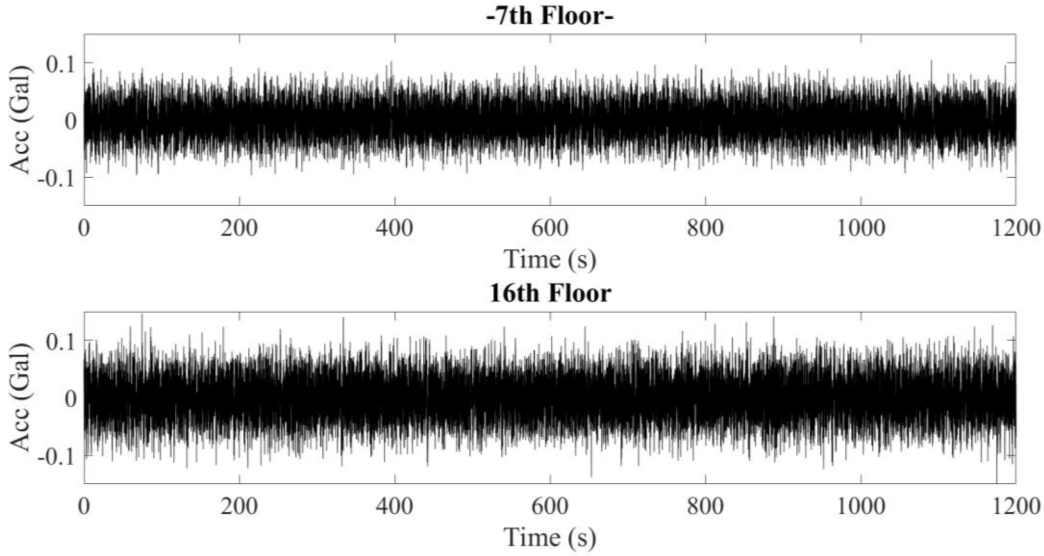

Figure 2.10 : Representative ambient vibration data on the -7th and 16th floor in EW direction.

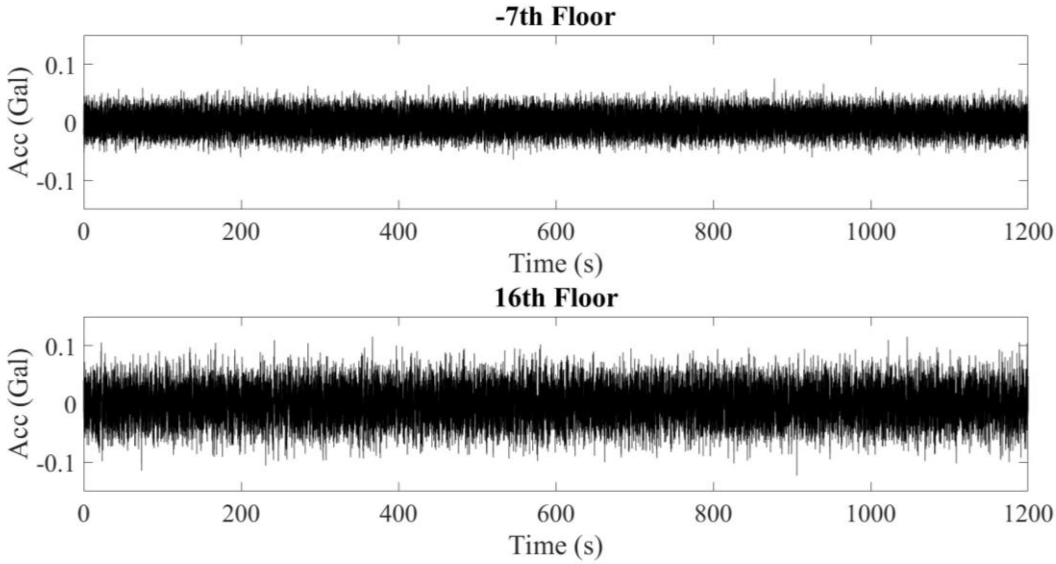

Figure 2.11 : Representative ambient vibration data on the -7th and 16th floor in NS direction.

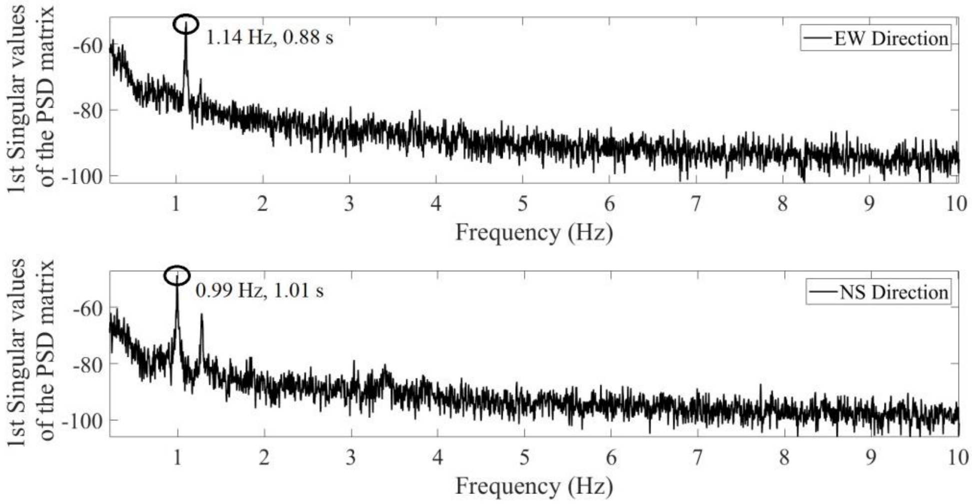

Figure 2.12 : FDD of before the earthquake ambition records in both directions.

Before the earthquake, a total of 10 more ambient vibration data are also analyzed, represented in Table 2.2.

Table 2.2 : The results of 10 more ambient vibrations before the earthquake.

No	Date	Initial Time/ Duration (min)	Period (s) EW Dir.	Period (s) NS Dir.
1	July 5, 2019	02:00 / 20	0.87	1.00
2	July 5, 2019	04:00 / 20	0.87	1.00
3	July 15, 2019	04:00 / 20	0.89	1.01
4	July 25, 2019	02:00 / 20	0.88	1.00
5	Aug 5, 2019	04:00 / 20	0.87	1.01
6	Aug 5, 2019 (Denizli Eq)	11:25 / <1	0.89	1.02
7	Aug 15, 2019	02:00 / 20	0.87	1.00
8	Aug 25, 2019	02:00 / 20	0.87	1.00
9	Sep 5, 2019	03:00 / 20	0.88	1.01
10	Sep 24, 2019 (Marmara Eq, Mw=4.4)	11:00 / <1	0.91	1.02

2.3.2 Investigation of response of the building under the Marmara earthquake

An earthquake with a magnitude of 5.8 struck southwest of Istanbul in the Marmara sea, Silivri deficits, on Sept. 26. The distance between the epicenter of the earthquake and the building is 73.72 km. Locations of the earthquake and the building can be seen in Figure 2.13. Besides, AFAD's stations [14] and their distance to the epicenter of the earthquake are shown in Figure 2.14. The comparison of the data taken from the accelerometer on the building during the earthquake and the records of the stations are presented in the Result chapter.

Figure 2.13 : The epicenter of the Earthquake and the Building with distance

The system is available to record data for 24 hours and 7 days a week, which enables to access specified time data and event data. Wave-forms of raw data of response of the building during the earthquake taken from the monitoring system are shown in Figure 2.15. Also, peaks of the raw data in the EW and NS directions are listed in Table 2.3.

Figure 2.14 : AFAD’s stations and their distance to the epicenter of the earthquake.

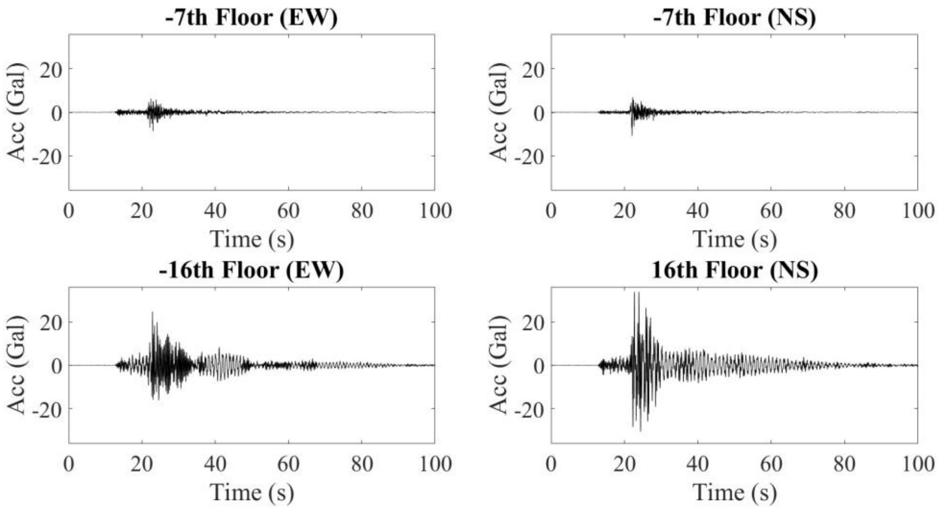

Figure 2.15 : Waveforms of the response of the building in EW and NS directions.

Table 2.3 : The peak of raw data of the response of the structure.

	Acceleration Peaks (Gal)	
	Base	Top
EW	-8.67	24.76
NS	-10.20	34.28

Response vibration of the structure during the earthquake is analyzed by FFT and PSD method in order to obtain the predominant frequency of the structure after the data acquisition. The methods are carried out via the Matlab platform. The fitting technique is applied to fix the transfer functions to the theoretical transfer function. According to analysis results, the transfer functions are estimated as shown in Figures 2.16 and 2.17.

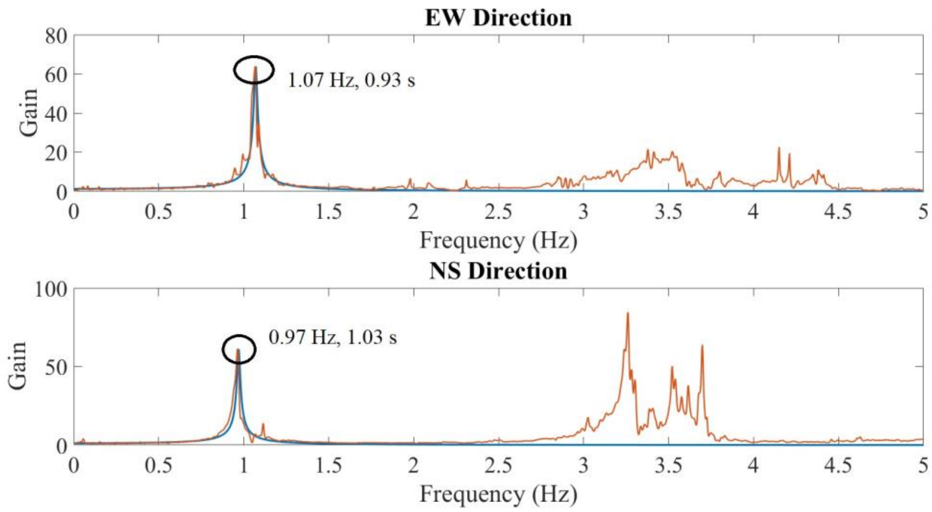

Figure 2.16 : Estimated transfer function in the EW and NS directions with the FFT method.

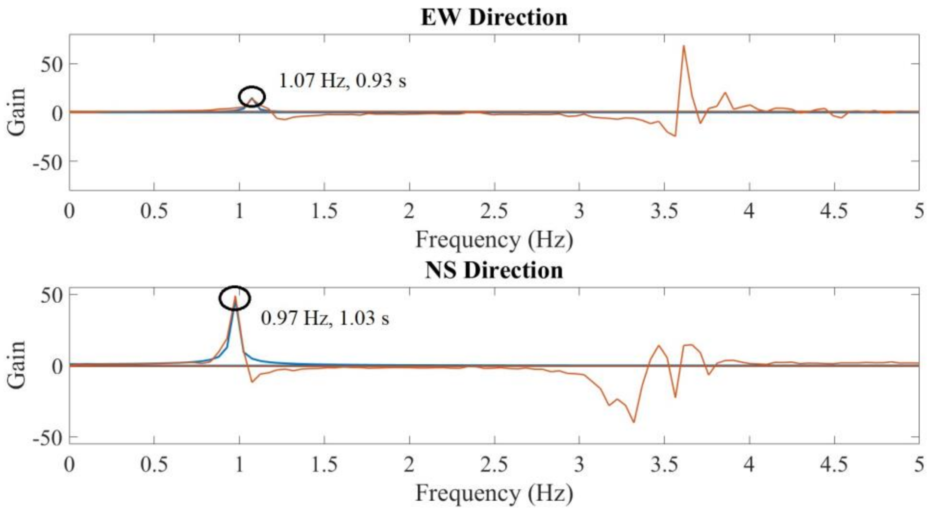

Figure 2.17 : Estimated transfer function in the EW and NS directions with the CPSD method.

The package program is also applied to the raw data to check the accuracy of the methods. SeismoSignal which is commonly known software is used. It is possible to calculate the Fourier spectra, velocity, and the displacement of the acceleration via the software. Moreover, SeismoSignal is capable of carrying out various filtering techniques and baseline correction.

The transfer function is also estimated by using the software. The results which are shown in Figure 2.18 indicate that there is no inconsistency of the methods to find the predominant frequencies of the structure.

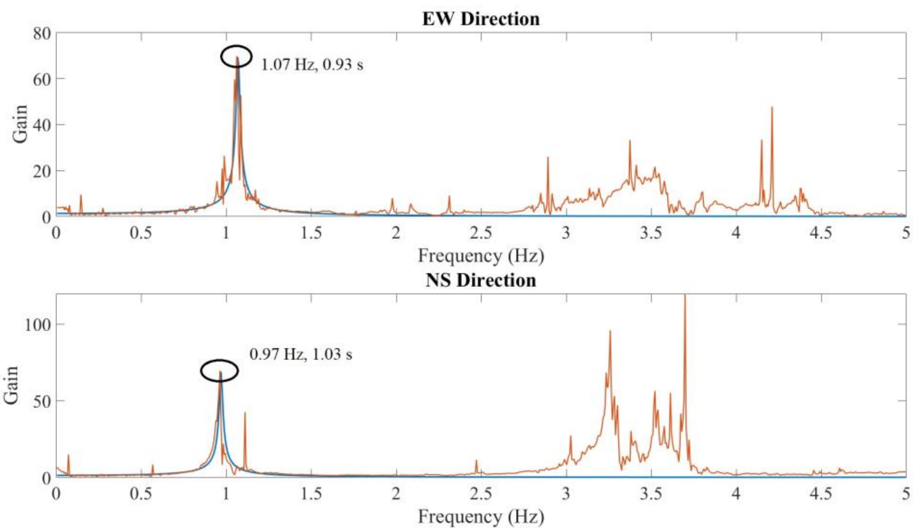

Figure 2.18 : Estimated transfer function in the EW and NS directions by SeismoSignal.

The peaks in Figures 2.16, 2.17, and 2.18 represent the predominant frequency in the EW and NS directions. The predominant period of the structure in the EW direction is found as 0.93 seconds while the first mode period is found out at 1.03 s. These results are also obtained from filtered and baseline-corrected data to check the possible noise effects on the data set. In this case, there are no differences in terms of predominant frequency in the EW and NS directions.

After calculating the predominant frequency of the structure under the earthquake, the acceleration, velocity, and displacement of the absolute response of the 16th floor are obtained from recorded acceleration. Firstly, the baseline correction and the filtering technique is applied to the raw data in order to remove the unwanted frequency components from the data. While the acceleration is integrated to calculate the velocity and the displacement, prevention from a cumulative accumulation of noise is needed. Therefore, corrected data is used for better results. A linear function ($y=a_0+a_1x$) is applied for the baseline correction. The importance of the baseline process is well noticeable in the displacement time history which is obtained from double integration of both the uncorrected and corrected data. Secondly, the 4th order band-pass Butterworth filtering technique is applied with corner frequencies which are 0.10 Hz and 25 Hz.

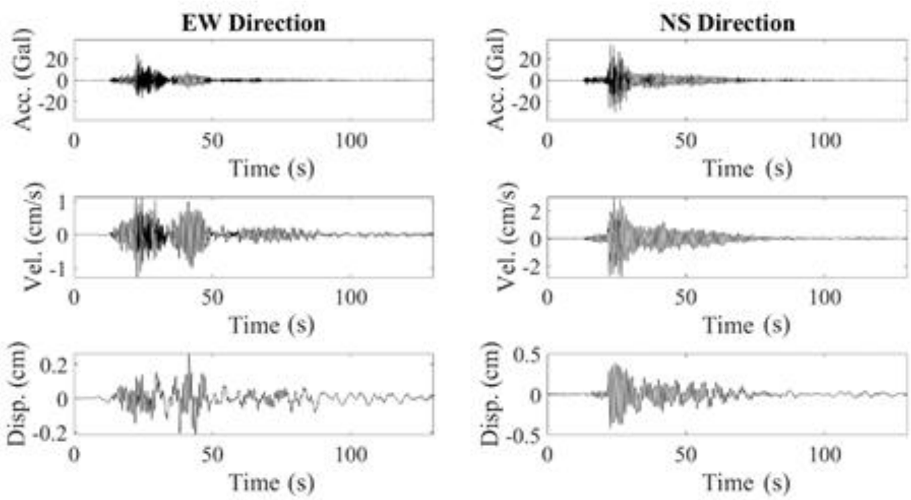

Figure 2.19 : The filtered time histories of acceleration, velocity, and displacement of the 16th floor in EW and NS directions obtained by Matlab code.

Finally, acceleration, velocity, and displacement time histories are obtained from the data after removing the noise. In addition to this conventional signal processing method, 4th order B-spline mother wavelet is applied to decompose the signals and to eliminate the noise from the raw data. The results of both methods are shown in Figures 2.19 and 2.20.

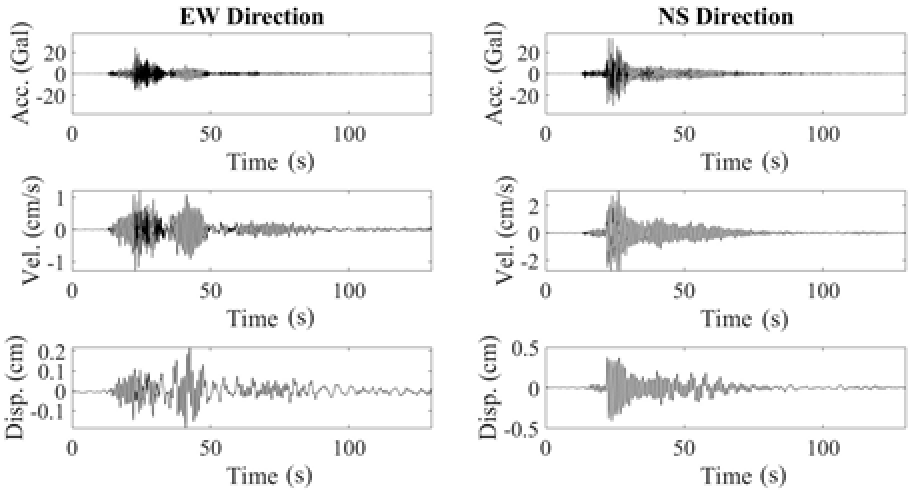

Figure 2.20 : The filtered time histories of acceleration, velocity, and displacement of the 16th floor in EW and NS directions obtained by Wavelet Transform.

To control the results of the techniques, SeismoSignal is also used. The results obtained from SeismoSignal can be seen in Figure 2.21. Table 2.4 and Table 2.5 demonstrate the results of all peak values of the acceleration, velocity, and displacement on the 16th floor of the building in the EW and NS directions for each analysis.

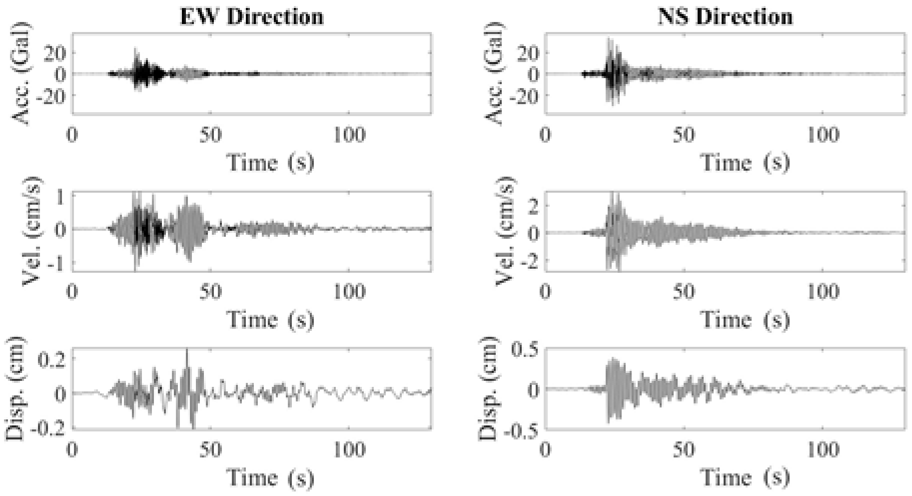

Figure 2.21 : The filtered time histories of acceleration, velocity, and displacement of the 16th floor in the EW and NS directions obtained by SeismoSignal.

Table 2.4 : Comparison of the results of acceleration, velocity, and displacement peak values obtained by Matlab code, WT, and SeismoSignal for EW direction.

	Absolute Maximum Values		
	Acceleration (Gal)	Velocity (cm/s)	Displacement (cm)
Matlab Code	24.76	1.28	0.26
WT	24.50	-1.29	0.22
SeismoSignal	24.77	-1.28	0.26

Table 2.5 : Comparison of the results of acceleration, velocity, and displacement peak values obtained by Matlab code, WT, and SeismoSignal for NS direction.

	Absolute Maximum Values		
	Acceleration (Gal)	Velocity (cm/s)	Displacement (cm)
Matlab Code	24.76	1.28	0.26
WT	24.50	-1.29	0.22
SeismoSignal	24.77	-1.28	0.26

2.3.3 Ambient vibration after the earthquake

Ambient vibration record is taken after the Marmara earthquake in order to examine whether there is a change in the dynamic properties of the building after the earthquake or not. The record is selected at between 02:55 and 03:10 am on the date of 09 October 2019. The time interval, which contains the cleanest record, is chosen since the building is in use and the ambient vibration data can be easily contaminated. The representative ambient vibration records are taken from the -7th and 16th floor of the building for both EW and NS directions are presented in Figures 2.22 and 2.23, respectively.

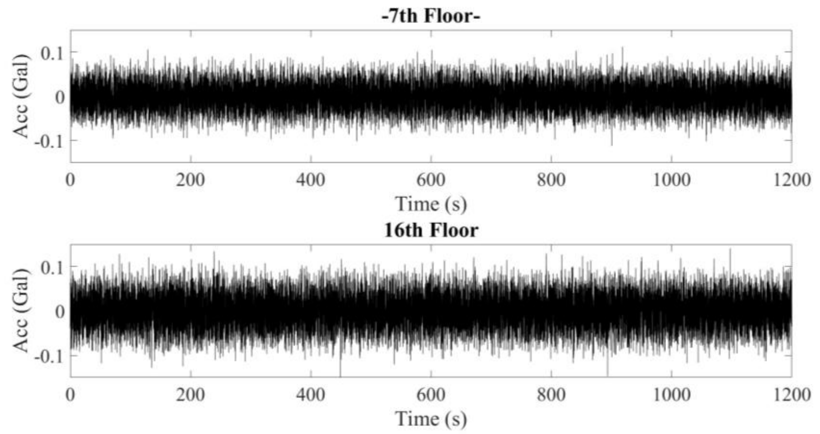

Figure 2.22 : Representative ambient vibration data on the -7th and 16th floor in EW direction.

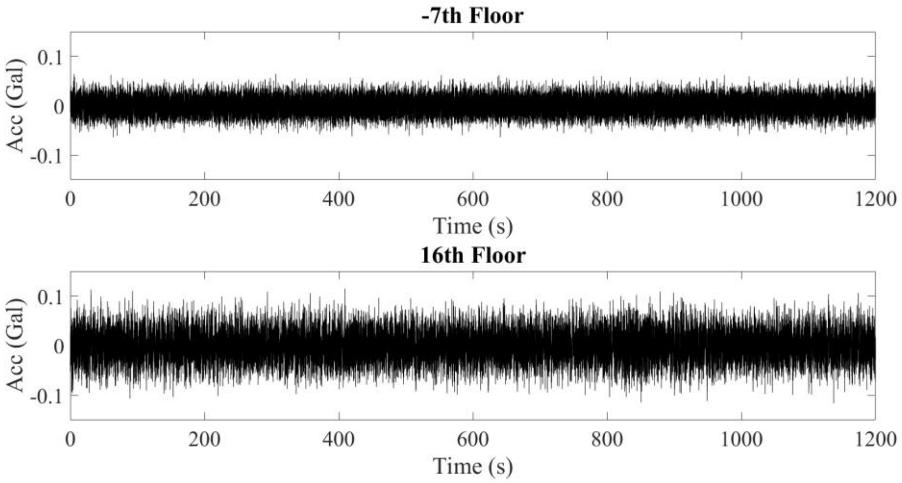

Figure 2.23 : Representative ambient vibration data on the -7th and 16th floor in NS direction.

Ambient vibration responses are analyzed by the FDD method after the data acquisition. Figure 2.24 shows the results of the analyses. The first mode period is found out at 0.93 s for EW direction while a peak in the NS direction identifies the predominant periods at 1.03 s.

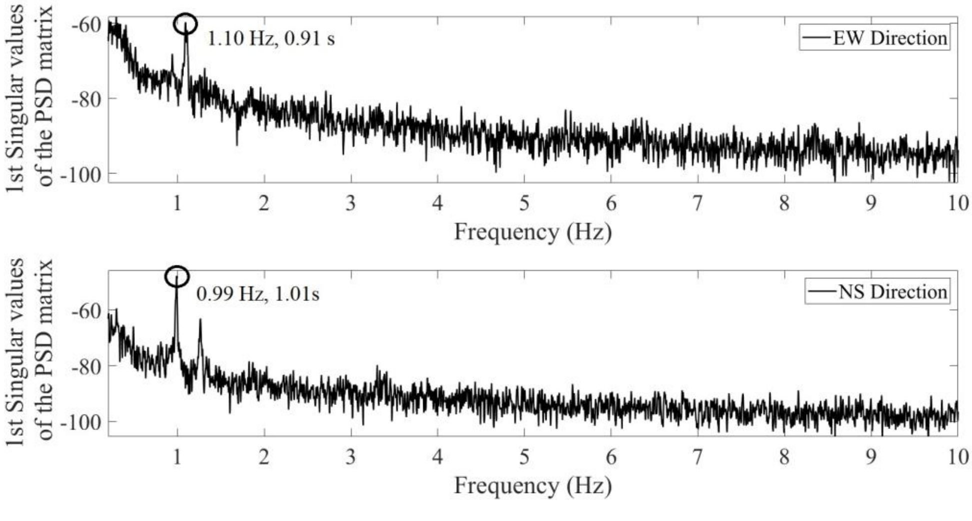

Figure 2.24 : FDD of after earthquake ambition vibration records in both directions.

Additionally, the ambient vibration data is recorded between 21:10 am and 21:30 am on the date of October 28, 2019. Data is gathered by SENSEBOX703X. The five accelerometers are located in -5F, -1F, 7F, 12F, and 16F on the building. Identified modal periods of the building can be seen for EW and NS directions in Table 2.6. Additionally, the analyses results and mode shapes of the building are demonstrated in Figure 2.25 and Figure 2.26, respectively.

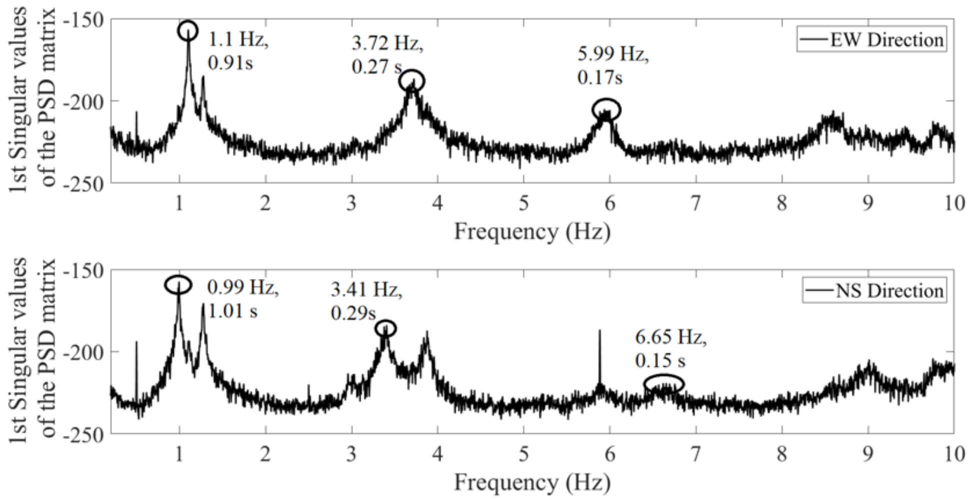

Figure 2.25 : Model frequencies and periods of the building in both directions.

Table 2.6 : Identified modal periods of the structure.

	Modal Periods (s)		
Direction	1st	2nd	3rd
EW	0.91	0.27	0.17
NS	1.01	0.29	0.25

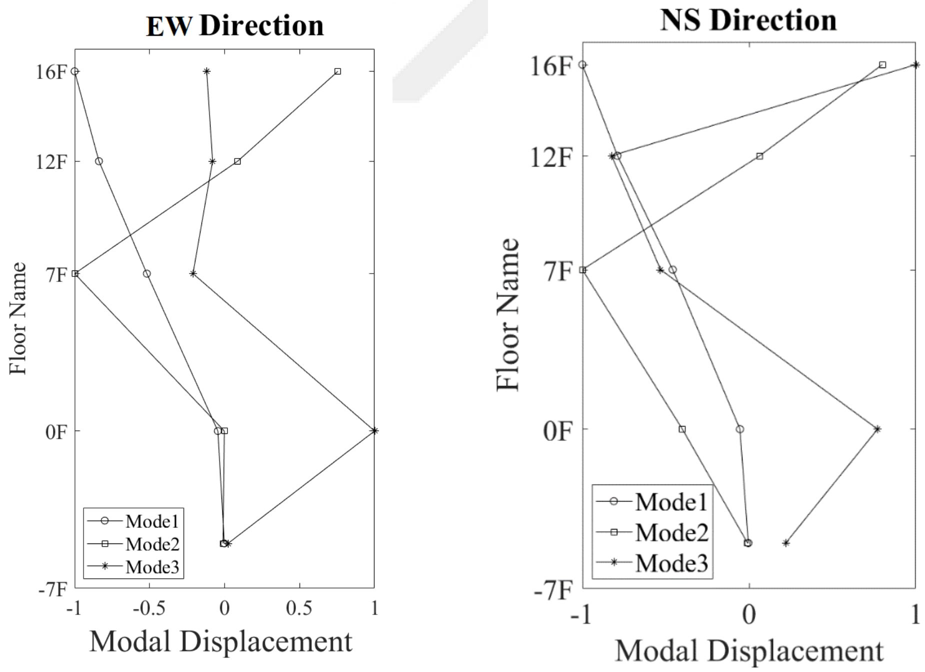

Figure 2.26 : Mode shapes of the building in both directions.

After the earthquake, 23 more ambient vibration data are also analyzed, represented in Table 2.7.

Table 2.7 : The results of 23 more ambient vibrations before the earthquake.

No	Date	Initial Time/ Duration (min)	Period (s)	
			EW Dir.	NS Dir.
1	Sep 28, 2019	04:00 / 20	0.90	1.01
2	Sep 29, 2019	04:00 / 20	0.90	1.01
3	Oct 5, 2019	04:00 / 20	0.89	1.01
4	Oct 9, 2019	02:00 / 20	0.91	1.01
5	Oct 10, 2019	04:00 / 20	0.91	1.01
6	Oct 20, 2019	02:00 / 20	0.90	1.01
7	Nov 10, 2019	04:00 / 20	0.90	1.01
8	Nov 20, 2019	02:00 / 20	0.92	1.01
9	Dec 10, 2019	02:00 / 20	0.91	1.01
10	Dec 20, 2019	02:00 / 20	0.90	1.01
11	Jan 10, 2020	02:00 / 20	0.90	1.01
12	Jan 11, 2020 (Manisa Eq.)	16:36 / <1	0.93	1.02
13	Jan 20, 2020	04:00 / 20	0.91	1.01
14	Feb 10, 2020	02:10 / 30	0.91	1.01
15	Feb 20, 2020	02:00 / 20	0.91	1.02
16	Mar 10, 2020	02:00 / 20	0.91	1.02
17	Mar 20, 2020	02:00 / 20	0.92	1.01
18	Apr 10, 2020	02:00 / 20	0.91	1.01
19	Apr 20, 2020	02:00 / 20	0.92	1.02
20	Apr 25, 2020	04:00 / 20	0.92	1.02
21	May 1, 2020	02:00 / 20	0.88	1.01
22	May 2, 2020	02:00 / 20	0.88	1.01
23	May 3, 2020	02:00 / 20	0.88	1.01

3. FINITE ELEMENT MODEL (FEM) OF THE BUILDING

In this chapter, the existing high-rise building is examined analytically. The building consists of 25 stories in total. Beams, columns, slabs, and shear walls exist on the building as structural elements. A temporary sheet wall system was used during the construction of the building. Currently, the building is available for active usage, therefore there are non-structural elements in the building. The building was designed mainly based on the Turkish Seismic Design Code (2007). The modal analyses are applied to each FE model of the building in order to find their modal parameters. The building shows linear behavior during the earthquake according to the result of SHM. Thus, the linear time history analyses are carried out by applying input recorded by the accelerometer on the -7th floor. The input data are executed for each FE model of the building.

3.1 Overview of the Building

In this study, the building is investigated both experimentally and analytically. Structural and dynamic analyses are carried out with the use of commercial FEM software, ETABS v.16.0.0.

The building consists of 25 stories, 7 of which are basement floors, and 1 of which is ground and roof-top floors. The height of the building is 82.8 m. The floor heights are 3.30 m, 3.40 m, 3.80 m, 4.50 m on the basement floors, 4.22 m on the ground floor, 3.20 m on the roof-top floor, and 3.12 m for the rest. The reinforced concrete system consists of slabs, beams, columns, and shear walls. The name and altitude of the floors are demonstrated in Table 3.1.

The building consists of mainly 3 different key plans which change with respect to story levels: from -7F to the 0F, from 0F to 16th floor, and the top of the building. Figure 3.1 shows the key plans altogether. In Figure 3.2, the key plan of the infill which is used between 0F to 16F can be seen. Autoclaved aerated concrete (AAC) infill walls are used in the building. In the figure, red, blue, and green marked walls present the width of the walls of 20 cm, 15 cm, and 10 cm, respectively. Additionally, black marked walls on the key plan are ignored in the model.

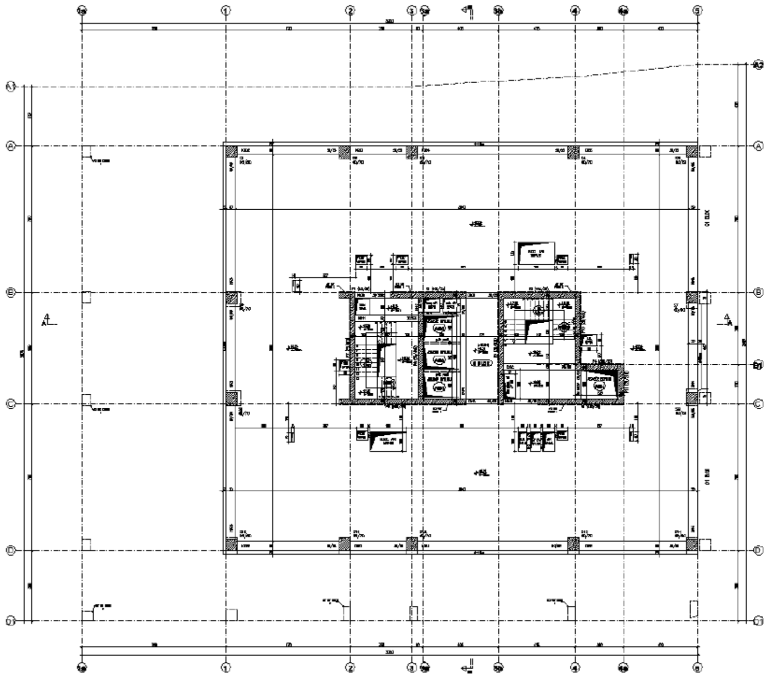

Figure 3.1 : The key plan of the building.

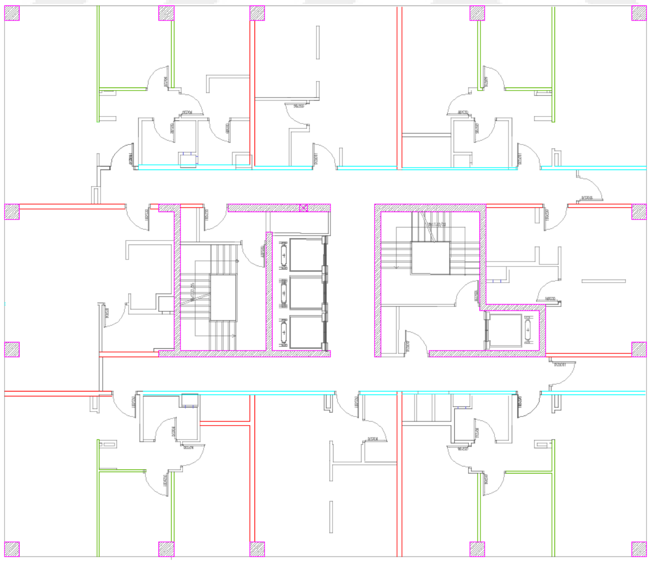

Figure 3.2 : The key plan of the infill walls used in the building.

There are 10 columns, 16 beams, 3 slabs, and 6 shear walls whose dimensions are changing on different floors. All structural elements for each floor are modeled. Size of the shear walls changes from 25 cm to 50 cm. The weakest column type is 50 cm*60 cm and the strongest one is 100 cm*80 cm. The width of the flat slabs has 28 cm. and the rest of the slabs has 18 cm.

The material properties which are used on the design stage are;

- Modulus of elasticity and class of concrete: C40, E = 34000 MPa,
- Poisson's ratio and Shear modulus of concrete: 0.2, G = 13600 MPa,
- Modulus of elasticity and class of steel: B420C, E = 200000 MPa,
- Poisson's ratio and Shear modulus of steel: 0.3, G = 76903 MPa,

Table 3.1 : Name, elevation, and height of each story.

Name of Story	Height (m)	Altitude above sea level (m)
Top	3.20	112.04
16F	3.12	108.84
15F	3.12	105.72
14F	3.12	102.60
13F	3.12	99.48
12F	3.12	96.36
11F	3.12	93.24
10F	3.12	90.12
9F	3.12	87.00
8F	3.12	83.88
7F	3.12	80.76
6F	3.12	77.64
5F	3.12	74.52
4F	3.12	71.40
3F	3.12	68.28
2F	3.12	65.16
1F	3.12	62.04
0F	4.22	58.92
-1F	3.80	54.70
-2F	3.50	50.90
-3F	3.50	47.40
-4F	3.50	43.90
-5F	4.50	40.40
-6F	3.30	35.90
-7F	3.40	32.60
Base	-	29.20

The seismic parameters which are classified according to TSC-2007 are;

- Site Class: Z1,
- Seismic Zone and Effective Ground Acc. Factor: 1, 0.4,

- Building Importance Factor, I: 1.0,
- Structural system behavior factor, R: 6.

The building has a mat foundation of which sectional depth is 150 cm. Comparison has been carried out with and without foundation modeling. Then, it is seen that the foundation does not affect the dynamic characteristic of the building due to soil conditions. Therefore, the building is modeled with fixed support instead of a mat foundation to reduce analysis time. Besides, the shear walls and floor slabs are modeled as a shell element. In addition, the slabs are modeled without using a diaphragm. The beams are represented with frame-type members in the 3D-model shown in Figure 3.3.

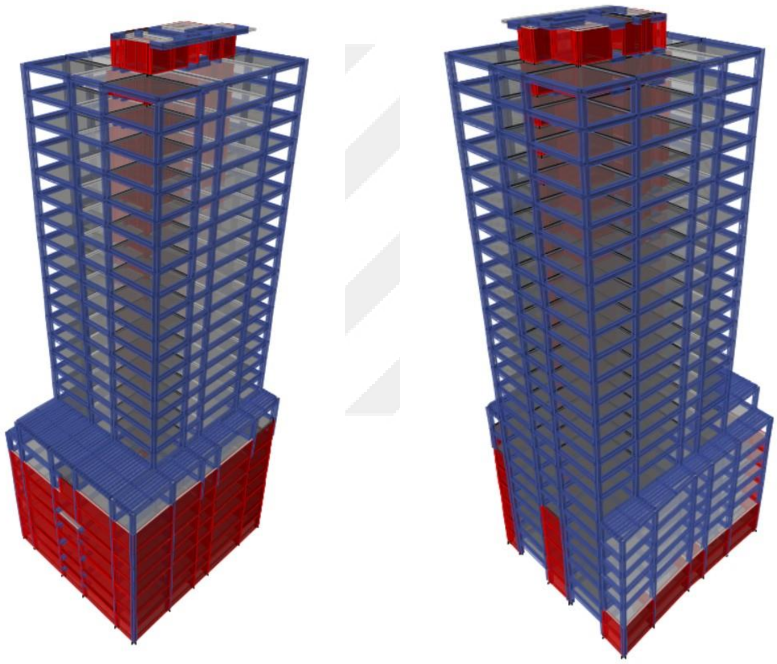

Figure 3.3 : 3D model of the building with 4 sides.

The foundation and the shear walls which surround the building are located under the ground levels. Since there is an interaction between the building and the soil, information about soil condition is expressed below. This information is taken from the geotechnical report.

- Modulus of vertical subgrade reaction is 600000 kN/m^3,
- Modulus of horizontal subgrade reaction is 1200000 kN/m^3, and
- Allowable soil stress is 700 kN/m^2.

Table 3.2 : The live and the additional loads used during the design phase of the building.

Load Distribution			
Slabs	Live Load (kN/m^2)	Finishing Load (kN/m^2)	Wall Load (kN/m^2)
-7F to -2F	5.0	0.240	-
-2F to 0F	3.5	0.240	1.0
0F to Top	3.5	0.235	1.0
Ramp	10.0	2.400	-
Ribbed	3.5	2.350	1.0

Weights of the structural elements are automatically calculated by the packaged software and applied to the structural system. In addition, live loads are applied with reduction factors. The reduction factor of 0.6 is used for live loads applied to slabs between the -7F and -2F. On the other hand, the reduction factor of 0.3 is used for the rest live loads applied to structure during the design phase modeling. Then, additional loads are calculated manually and applied to the system. The loads which are listed in Table 3.2 are considered in the design phase of the structure.

The thickness of the slabs and size of the columns, beams, and shear walls are changing with respect to stories. There are 10 columns, 16 beams, 3 slabs, and 6 shear walls whose dimensions are changing on different floors. All structural elements for each floor are modeled.

3.2 Procedures of Correcting FEM of the Building

3.2.1 Modeling of infill walls

The infill walls are commonly used as a partition wall in buildings. They are capable of separating the interiors from each other and cutting the connection between the building and the environment. Due to its different features, it also provides insulation of the buildings. The walls are consist of not only brick (or autoclaved aerated concrete (AAC)) blocks but also finishing elements such as mortar. The conjunction of these elements results in the strength and stiffness of these walls. However, the effects of these non-structural elements on the structure are much less than the structural elements relatively. While structural analysis is carried out, just modeling of the structural elements is most commonly used. The strength and stiffness of the non-structural elements are generally ignored in the structural analysis. Even though the effects of the infill wall panels on the rigidity of the structure are considered as reserve capacity, the distribution and the ratio within the floor of the walls may cause some problems such as torsional irregularity, short column, weak floor irregularity, and soft floor irregularity. Therefore, the masonry partition walls are studied experimentally and analytically by many researchers. These studies show that the contribution of the infill walls to the lateral strength and stiffness of the structure cannot be neglected especially for high rise buildings.

On the other hand, the walls are only considered as vertical loads for structural analyses in the current package software. Thus, many studies are focused on developing empirical equations, assumptions, and coefficients to enable modeling via package software. Macro and micro modeling methods are available in the literature.

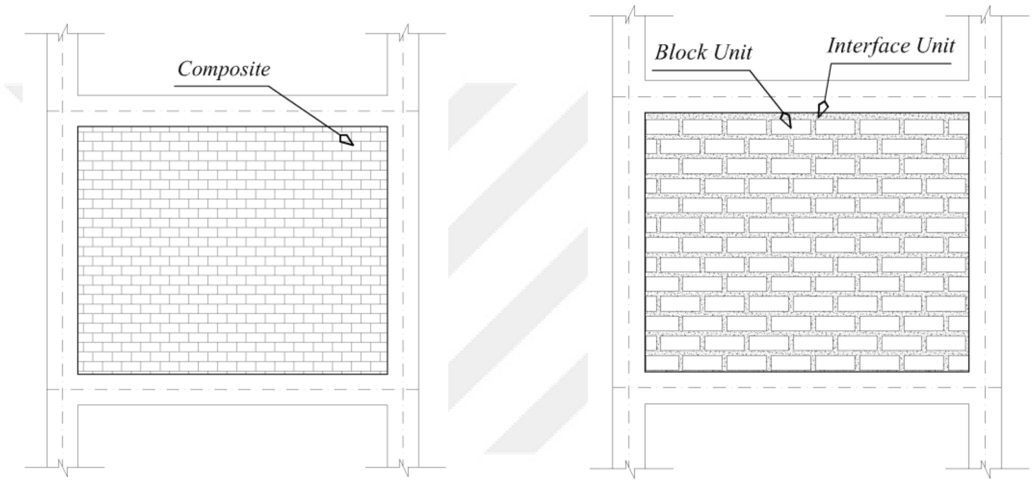

Figure 3.4 : Macro and micro modeling.

The masonry infill walls consist of more than one material that has various material properties. Macro modeling is based on considering the materials as a homogeneous single material. On the contrary, if these materials are modeled separately, this is called micro modeling. The draft of these modeling types can be seen in Figure 3.4. In the literature, the equivalent compressive strut and the finite element method are widely used for modeling infill walls.

3.2.1.1 Equivalent strut modeling

The main advantage of this method depends on its simplicity for computational purposes. When horizontal load effects to an infill wall on a floor alignment, it is assumed that the infill walls act as a compressive strut between the node influenced by load and its diagonal. The behavior of the equivalent strut and its geometry can be seen in Figure 3.5. This approach was first proposed by Polyakov, then it is mainly developed by Holmas, Smith, and Mainstone. The thickness of the strut equals to the thickness of the infill walls. Nowadays, some seismic design codes such as TSDC 2018 and FEMA 306 defines assumptions and formulas (equations 3.1 and 3.2) for equivalent compressive struts, which are given below.

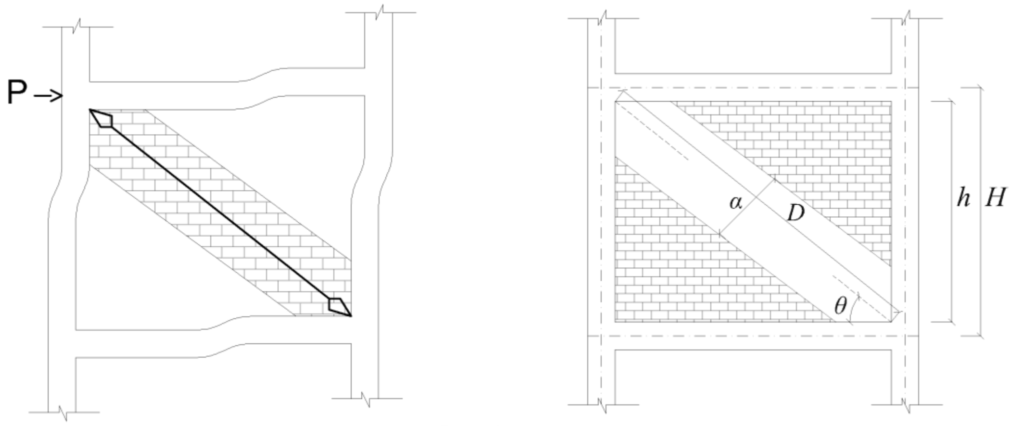

Figure 3.5 : Equivalent strut behavior and geometry.

$$a = 0.175D(\lambda_1 H)^{-0.4} \tag{3.1}$$

$$\lambda_1 = \sqrt[4]{\frac{E_m t sin2\theta}{4E_c I_{col} h}} \tag{3.2}$$

Where a, D, E_m, t, θ, E_c, I_{col}, H and h represent the equivalent width of infill strut (cm), relative infill to frame stiffness parameter, the modulus of elasticity of masonry infill (MPa), the gross thickness of the infill, angle of the concentric equivalent strut (cm), modulus of elasticity of confining frame (MPa), the moment of inertia of masonry infill (cm^4), the height of the confining frame (cm), and height of the infill (cm), respectively.

3.2.1.2 Modeling the infill walls as a shell element

The infill walls can be modeled as a shell element in addition to modeling as a frame element since the thickness of the infill walls is smaller than the other two dimensions relatively. In this method, the infill walls mesh into lots of small elements which are called finite elements. These elements can be modeled in detail by means of mortar or as a composite element. Micro models are mostly modeled with non-linear elements in order to obtain more realistic results. Although this modeling significantly increases precision, it also raises the analysis time. On the other hand, when the infill wall is modeled with macro model, then less information will be obtained from analyses. However, it may be suitable for modeling structures with large infill walls without detailed stress analysis.

One of the issues to be considered in modeling the filling walls as shell elements is the interface elements between the infill wall and the wall-frame. Since, when large displacements occur in the structure, the infill walls do not behave monolithically. Therefore, the interface element needs to define the connection between the infill wall and the frame. In the literature, some empirical relations have been developed for the interface elements. In one of these studies, the following empirical relations (equations 3.3 and 3.4) are obtained [15]. Figure 3.6 demonstrates the framed infill walls with interface elements.

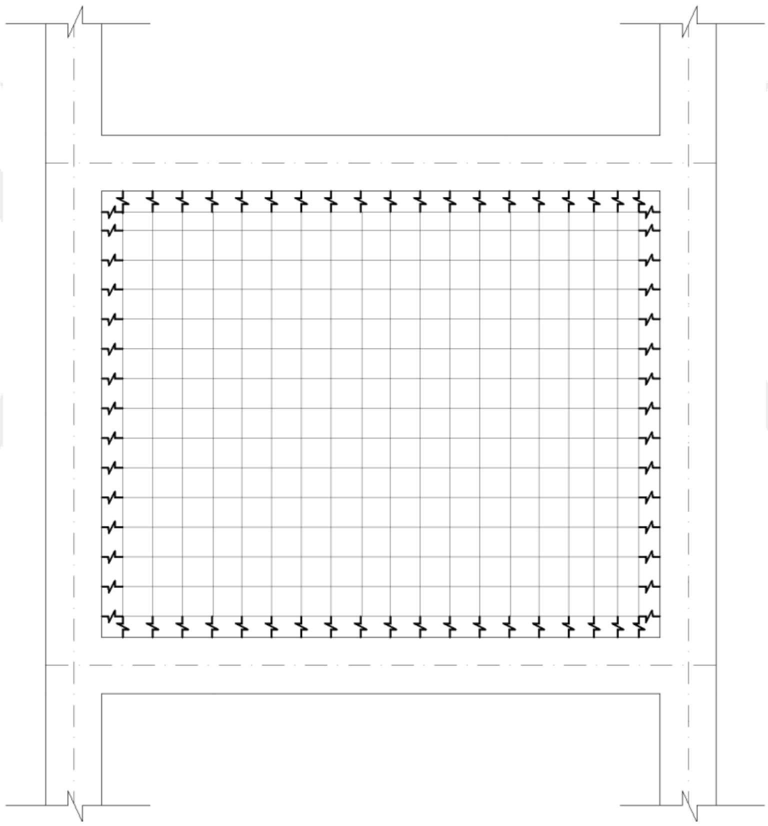

Figure 3.6 : Frame, infill, and interface elements.

$$k_i = t_{inf} E_{me} \tag{3.3}$$

$$k_g = 0.0378\, k_i + 347 \tag{3.4}$$

Where k_i and k_g represent the stiffness of the infill wall and stiffness of the interface element, respectively.

The infill wall can be considered as a shell element in cases of ambient or small vibrations since the infill wall behaves as a monolithic wall until the connection between wall and frame fails. The building studied in this thesis displays linear behavior, therefore the infill walls are modeled as macro-shell elements without using any interface elements (Figure 3.7). The modulus of elasticity for AAC blocks is taken as 3000 MPa based on an experimental study conducted in Ankara, Turkey [16].

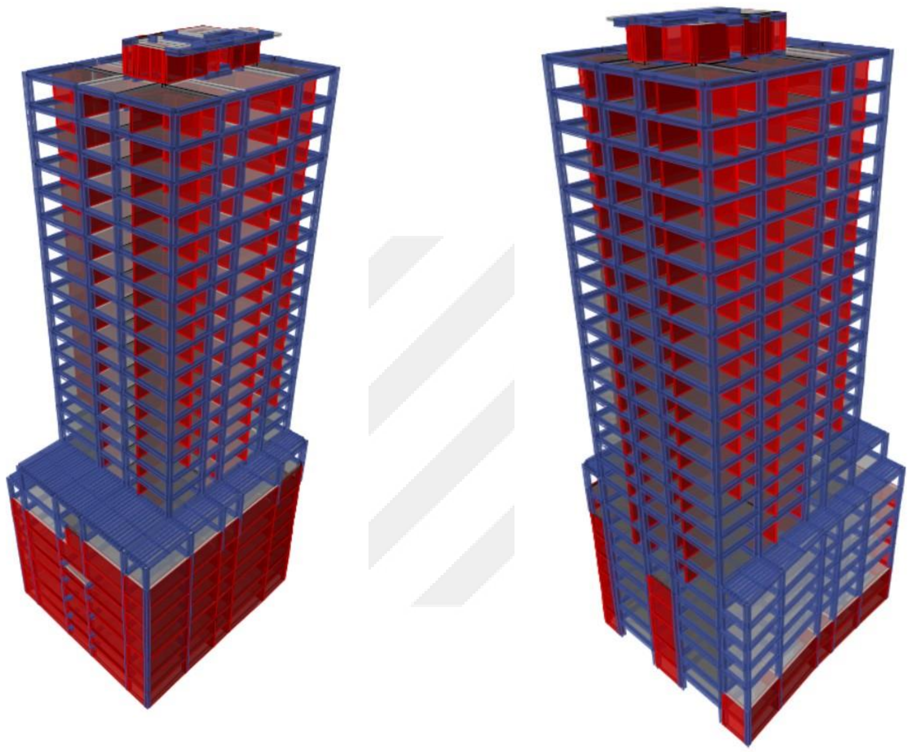

Figure 3.7 : 3D model of the building with infill walls around 4 sides.

3.2.2 Soil-structure interaction with underground stories

The effect of the earthquake on the structures is affected not only by the features of the superstructure but also by the interaction of the soil with the structure. By reflecting the effects of the behavior of the soil onto the structure, the effect of the soil-structure interaction can be taken into account. However, it is not easy to establish this relationship due to the complexity of the behavior displayed by the soil. The soil has a non-homogeneous structure and displays nonlinear behavior. In addition, the mechanical properties of the soil are affected by many factors such as its permeability and water saturation. Therefore, idealizations have been made despite this complexity of the soil.

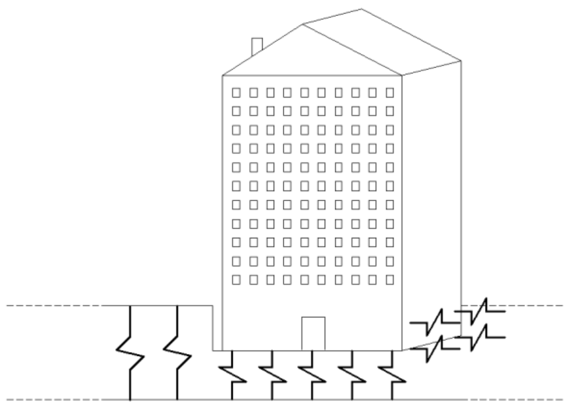

Figure 3.8 : Single parameter Winkler's Method.

The important study on the elastic behavior of the soil made by Winkler. Winkler's model (Figure 3.8), developed by Winkler, defines the soil behavior through springs that are infinitely close and linear elastic. These idealized springs have spring constants that depend on the displacement of the soil and the pressure at that point. It can be calculated by equation 3.5. These springs, which are infinitely close to each other, are considered to behave independently. Therefore, the behavior of a spring does not affect the other springs around it. Ignoring the interaction of the springs with each other can be seen as the biggest shortcoming of this model yet it also makes the modeling easier. In addition, the model can partially transfer the effects of the soil on the structure. Thus, it is possible to use the model in many structural systems. The report also suggests that horizontal spring can be used for embedded building with a basement surrounded by soil [17]. More modeling techniques were introduced by the NIST report in 2012 [17].

$$p(x,y) = kw(x,y) \tag{3.5}$$

Where $p(x,y)$, k, and $w(x,y)$ are pressure at a point (x,y), quantity characterizing the subgrade material, and deformation at a point (x,y).

In the scope of this thesis, since the building is subjected to a small vibration and its environmental vibration is examined, the soil effects can be applied by the springs on the shear walls surrounding the basements under the ground.

The coefficient of horizontal subgrade reaction of soil is 600000 kN/m^3. This coefficient is applied to the structure as a spring constant. The model which is created by affecting springs to the structural model with infill walls can be seen in Figure 3.9.

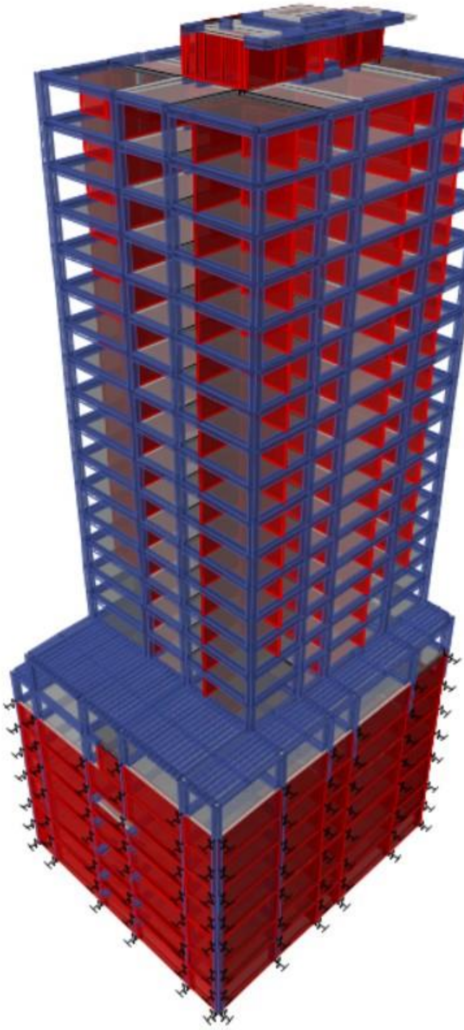

Figure 3.9 : 3D model of the structural system with infill walls and springs.

3.2.3 Half power bandwidth method for modal damping

The damping of structures can be calculated with different methods. The damping ratio of the structure can be estimated with a half-power bandwidth method which is one of the methods. This method is based on calculating the bandwidth for the resonance frequency of the structure to estimate the damping ratio. Figure 3.10 represents the half-power bandwidth method.

The resonance frequency can be defined as the oscillation of the system at the greatest amplitude. Since the damping ratio of the structures is generally less than 20%, the difference between resonance frequency and natural frequency remains insignificant. Therefore, the natural frequency of the structure can be used instead of the resonance frequency of the structure. This frequency can be obtained from ambient or forced vibration records of an acceleration time history. Equations 3.6 and 3.7 are used for the half band method [18].

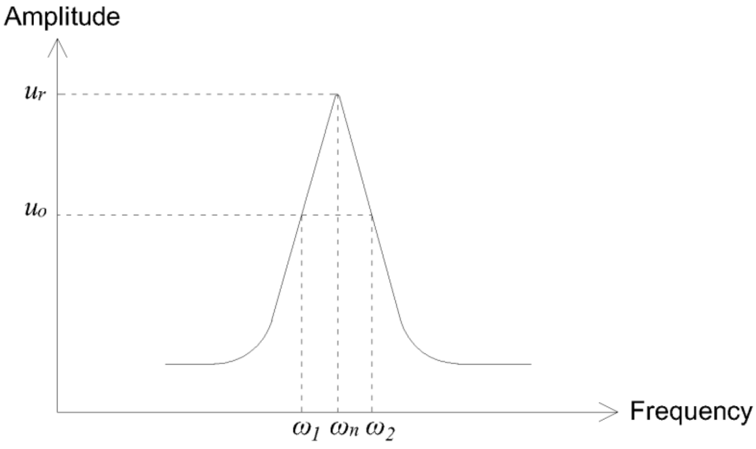

Figure 3.10 : Half power bandwidth method.

$$u_o = \frac{u_r}{\sqrt{2}} \tag{3.6}$$

$$2\xi = \frac{\omega_1 - \omega_2}{\omega_n} \tag{3.7}$$

Where u_o is $1/\sqrt{2}$ times the resonant amplitude, u_r. ω_2 and ω_1 are the forcing frequencies on either side of the resonant frequency at which u_o. ωn represents the natural frequency of the system.

3.3 Analyses Results of FEM

In addition to experimental determination, modal analyses and the acceleration, velocity, and displacement response of the building during the earthquake are also calculated analytically. The results of the mathematical model which is created by ETABS2016 v16.0.0 are represented in the chapter. The structural model is corrected step by step considering the masonry infill walls and soil-structure interaction in order to have a more realistic mathematical model. Besides, the analytical model is also updated only chancing the elastic modules of the concrete strength on the structural model to provide the measured first natural period of the existing building in the NS direction. This model is named an "updated structural model" for the rest of the study.

The response of the structure is highly affected by the damping ratio. Therefore, calculated damping ratio based on experimental determination and suggested one according to TSDC 2018 are used for each model during the time-history analyses. According to the calculated damping ratio, the damping ratios are set as 1.4% in the EW direction and 0.9% in the NS direction. The suggested damping ratio is also set as 2.5% in both directions [19].

Modal analyses are carried out to calculate the natural periods of each FE modal. In addition, linear time history analyses are executed to all modal to obtain the absolute acceleration, velocity, and displacement of the structure on the 16th floor. Acceleration time-history record taken from the accelerometer on the -7th floor is executed as an input of the earthquake in the EW and NS directions. The input of the time history records can be seen in Figures 3.11 and 3.12 for EW and NS directions, respectively.

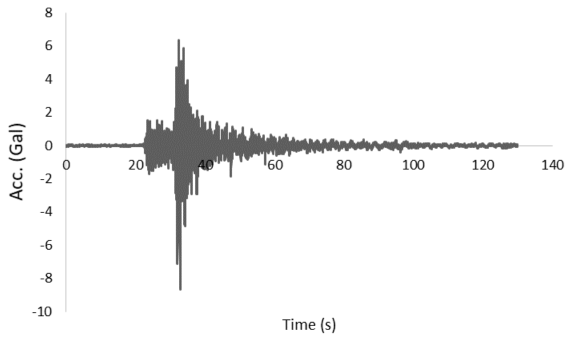

Figure 3.11 : Acceleration time-history record in the EW direction.

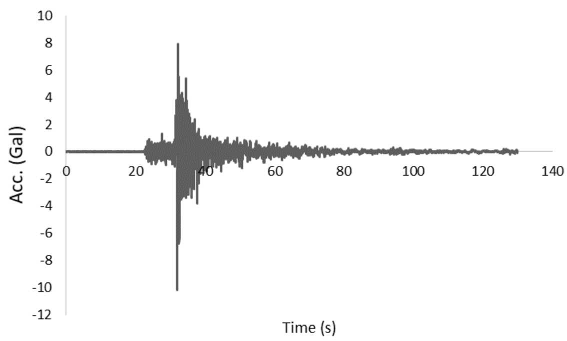

Figure 3.12 : Acceleration time-history record in the NS direction.

The American Concrete Institute (ACI) Code (2008) [20], Eurocode 2 (2005) [21], and Turkish Standards (TS-500) [22] provide different formulas such as equations 3.5, 3.6, and 3.7 for in the determination of elastic modulus of concrete. Only the Turkish Standards (TS 500) is used to calculate modulus of elasticity for concrete.

$$E_{cj} = 4700\sqrt{f_{cj}} \tag{3.5}$$

$$E_{cj} = 4700(f_{cj} + 8)^{1/3} \tag{3.6}$$

$$E_{cj} = 3250\sqrt{f_{cj}} + 14000 \tag{3.7}$$

Where E_{cj} and f_{cj} are the modulus of elasticity and the compressive strength of concrete, respectively.

C40 is used as the concrete class in the whole building. Reduced concrete strength is taken into consideration in order to remain on the safe state during the design phase of the buildings. Therefore, the elastic modulus and compressive strength of the concrete was taken as 34000 MPA and 40 MPa, respectively, while the building was designed. The result of the first natural periods of modal analyses of the structural design model are listed in Table 3.3.

Table 3.3 : The first three periods of the structural design model both directions.

Structural Design Model	
Direction	T (s)
EW	1.42
NS	1.86

The result of the model analyses of the structural design model resulted in a 53% error in the EW direction and 81% error in the NS compared to the experimental study. Hence, correcting the mathematical model is begun with correcting the strength of the concrete since concrete with higher concrete strength is used in order to ensure the safety of the structures, especially during the construction of high-rise buildings. TSDC 2018 considers this detail which reflects the reality in Turkey, thus the expected concrete strength of the existing high rise building is defined by the code. Equation 3.8 expresses the equation for expected concrete strength according to TSDC 2018 [19].

$$f_{cj} = 1.3f_{ck} \tag{3.8}$$

Where f_{ck} is the characteristic compressive strength of concrete.

Considering the expected concrete strength, compressive concrete strength of 52 MPa and 37500 MPa as elastic modulus of the concrete are used for each step of correcting the mathematical model of the structural model. Additionally, compressive concrete strength of 733 MPa and 102000 MPa of elastic modulus of the concrete is used for the updated structural mathematical model. After modification of the strength of the concrete, 2 kN/m^2 live loads are applied to each model with a 0.3 reduction factor. This assumption is made since the structure is not used with full capacity. Dead loads are also calculated by the software program automatically.

On the other hand, the additional wall load applied to the building during the design phase are investigated. The result of the calculation made for the wall load used in the existing building shows that the calculated wall load does not fit the applied load at the design phase. According to the calculation for wall load, additional wall load is applied with 0.35 kN/m^2 for each FE model of the building.

The result of the first three natural periods of modal analyses of each mathematical model is listed in Table 3.4.

Table 3.4 : Predominant periods of mathematical models.

	Predominant Periods (s)		
Slabs	T_1 (EW)	T_2 (NS)	$T_{torsional}$
Corrected structural model	1.32	1.71	1.21
Updated structural model	0.80	1.03	0.73
The structural model with infill walls	1.04	1.24	0.96
The structural model with infill walls and soil-structure interaction	0.98	1.12	0.95

The absolute acceleration, velocity, and displacement time history of the building on 16F are determined by time history analysis of the corrected structural model of the building for the calculated damping ratio, which is given by Figure 3.13.

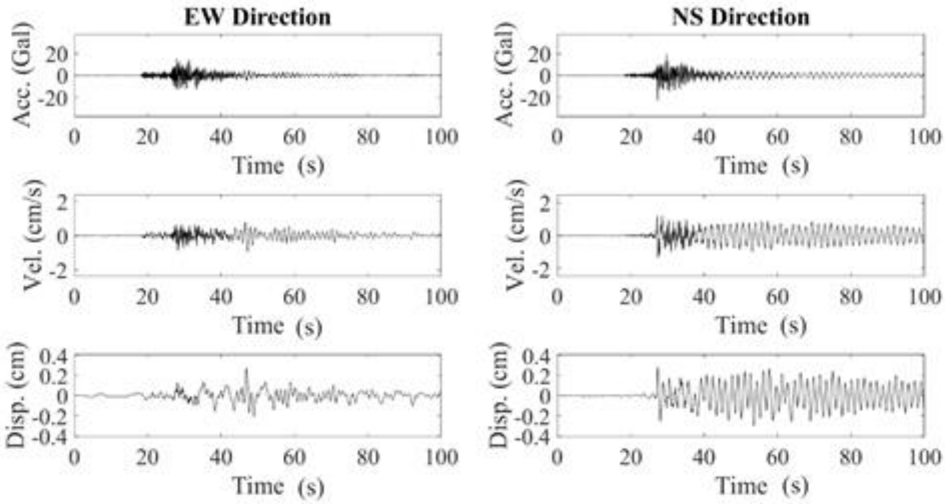

Figure 3.13 : The results of the time history analysis of the corrected structural model for 1.4% and 0.9% damping ratios in EW and NS, respectively.

The absolute acceleration, velocity, and displacement time history of the building on 16F are determined by time history analysis of the corrected structural model of the building for suggested damping ratio, which is given by Figure 3.14.

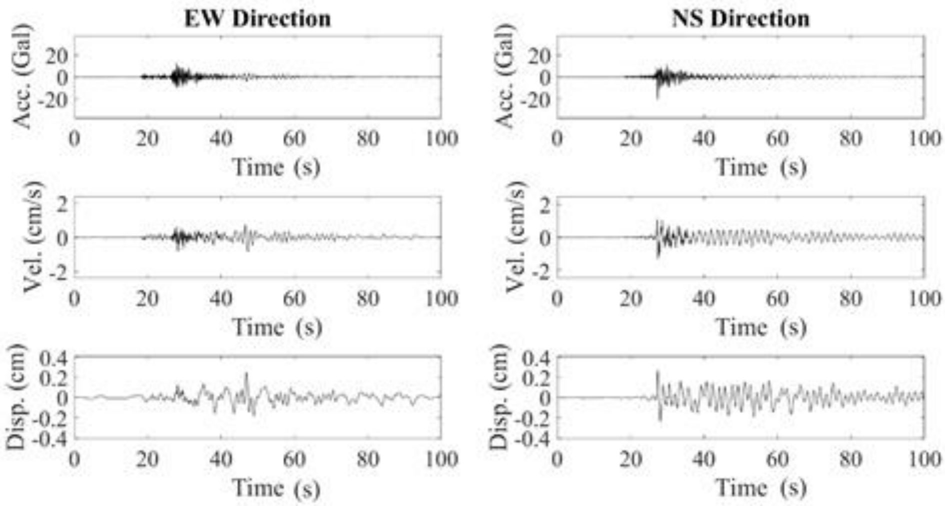

Figure 3.14 : The results of the time history analysis of the corrected structural model for 2.5% damping ratios in the EW and NS, respectively.

The absolute acceleration, velocity, and displacement time history of the building on 16F are determined by time history analysis of the structural model with only infill walls of the building for calculated damping ratio, which is given by Figure 3.15.

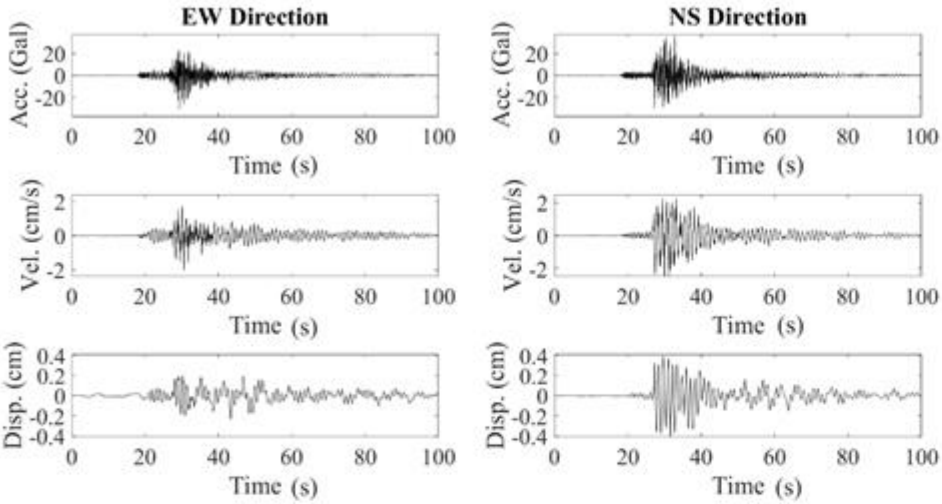

Figure 3.15 : The results of the time history analysis of the structural model with only infill walls for 1.4% and 0.9% damping ratios in the EW and NS, respectively.

The absolute acceleration, velocity, and displacement time history of the building on 16F are determined by time history analysis of the structural model with only infill walls of the building for suggested damping ratio, which is given by Figure 3.16.

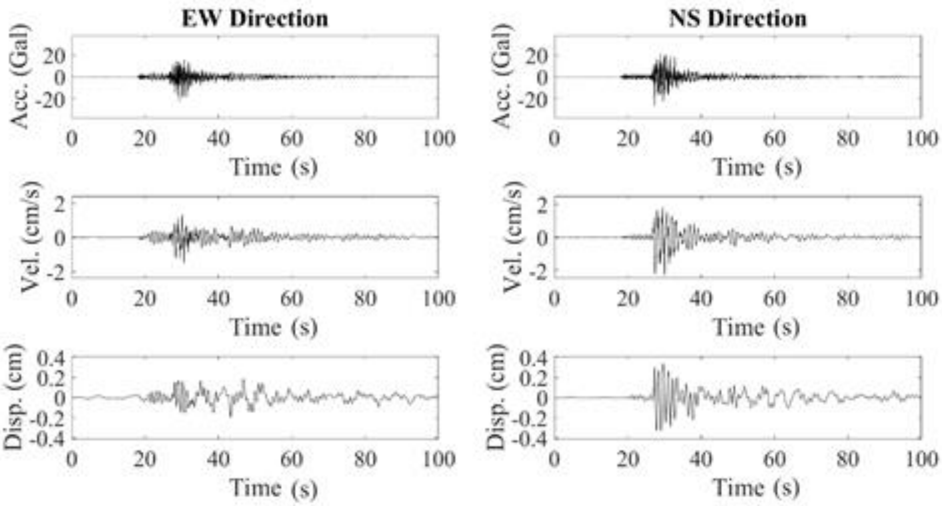

Figure 3.16 : The results of the time history analysis of the structural model with only infill walls for 2.5% damping ratios in the EW and NS, respectively.

The absolute acceleration, velocity, and displacement time history of the building on 16F are determined by time history analysis of the structural model with infill walls and soil-structure interaction of the building for calculated damping ratio, which is given by Figure 3.17.

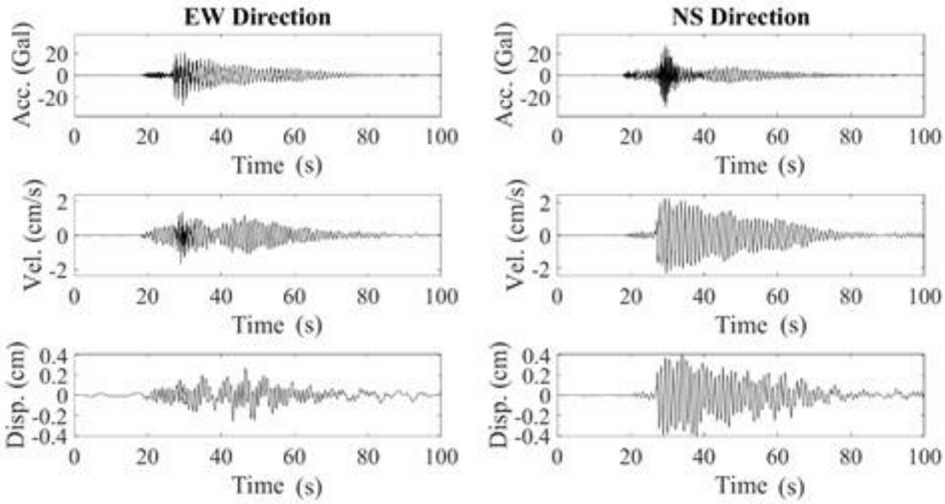

Figure 3.17 : The results of the time history analysis of the structural model with infill walls and soil-structure interaction for 1.4% and 0.9% damping ratios in the EW and NS, respectively.

The absolute acceleration, velocity, and displacement time history of the building on 16F are determined by time history analysis of the structural model with infill walls and soil-structure interaction of the building for suggested damping ratio, which is given by Figure 3.18.

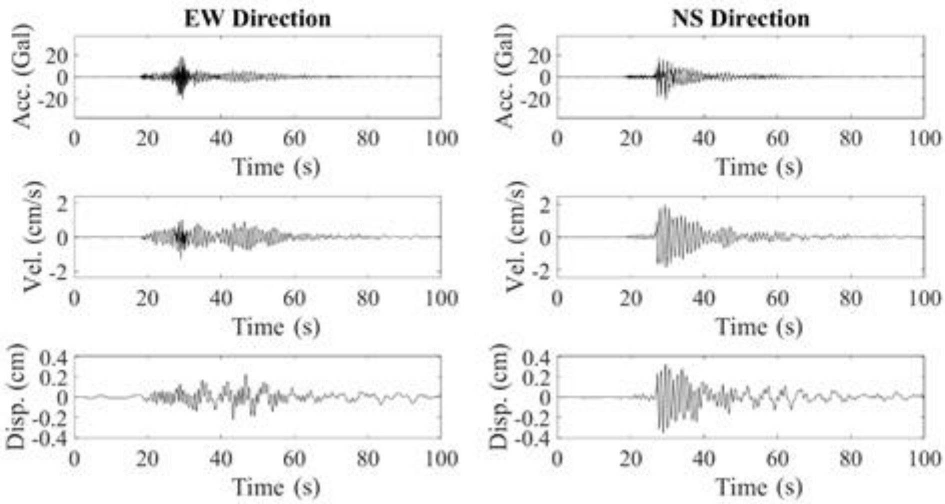

Figure 3.18 : The results of the time history analysis of the structural model with infill walls and soil-structure interaction for 2.5% damping ratios in the EW and NS, respectively.

The absolute acceleration, velocity, and displacement time history of the building on 16F are determined by time history analysis of the updated structural model the building for calculated damping ratio, which is given by Figure 3.19.

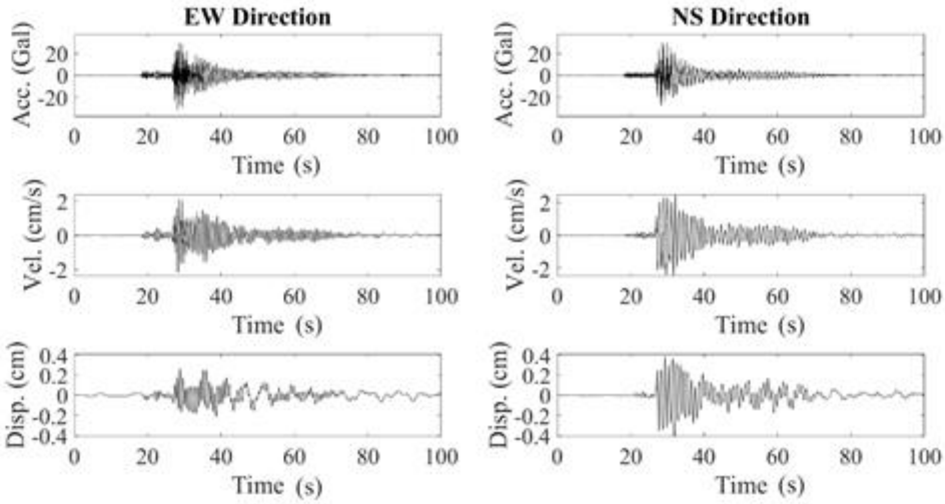

Figure 3.19 : The results of the time history analysis of the updated structural model for 1.4% and 0.9% damping ratios in the EW and NS, respectively.

The absolute acceleration, velocity, and displacement time history of the building on 16F are determined by time history analysis of updated structural model the building for suggested damping ratio, which is given by Figure 3.20.

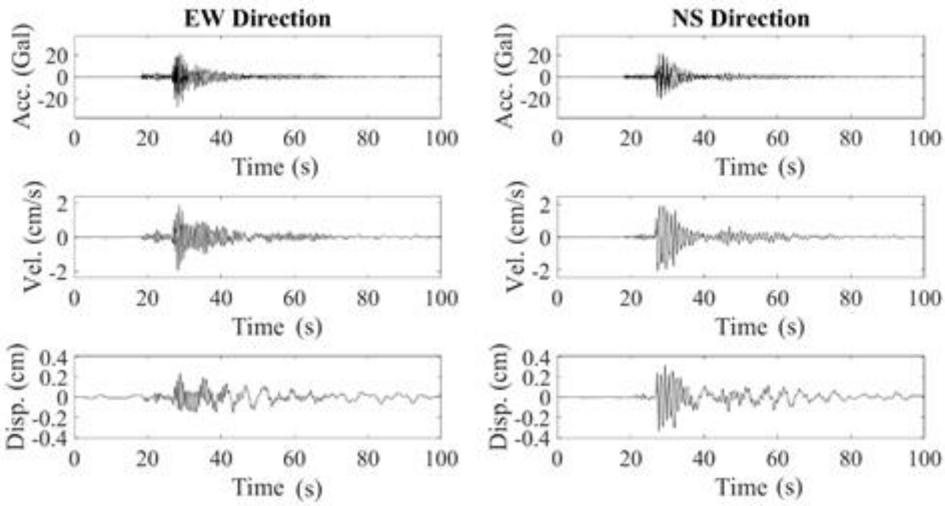

Figure 3.20 : The results of the time history analysis of the updated structural model for 2.5% damping ratios in the EW and NS, respectively.

The peak values of the results of time history analysis results are given in detail in the next chapter.

4. RESULTS

The main aim of the result section is to compare the results of both experimental study and FE models of the building. Therefore, the results of both system identification and modal analyses of the FE models of the building are compared. In addition, structural health monitoring and time history analyses of the building during the earthquake are also considered for this purpose. On the other hand, the comparison of the raw data recorded by the accelerometer located on the -7th floor of the building and the records of the AFAD's station [14] during the earthquake are presented. Moreover, the tensional concrete stress distribution of the critical locations of the building is shown.

First of all, the results of the monitoring of the building and the station are listed in Table 4.1 in order to investigate the accuracy of the data acquisition system. If the results of Umraniye station are taken as a reference, it can be seen that the station located farther away from the epicenter compared to the building has a higher amplitude of acceleration compared to the data acquisition system of the building. In that case, the effect of the shear velocity distribution of the soil needs to be considered, since Hermann and et al. showed that the region with low shear velocity distribution is exposed to high levels of damage during the earthquake [23]. Additionally, ground motion reduces with depth below the free surface therefore, embedded foundation below te ground face has reduced ground motions [17]. The studies explain the reason for the low amplitude of the acceleration recorded by the system on the building.

Table 4.1 : The raw data records of the building and stations.

Stations	Altitude (m)	$V_{s_{30}}$ (m/s)	Distance to Epicenter of the Eq. (km)	Peak Acc. of Raw Data (Gal) NS	EW	UD
Buyukcekmece	13	436	35	44.60	84.92	48.00
Fatih	34	323	66	43.12	39.56	19.72
Umraniye	148	247	81	31.39	28.70	15.39
Kartal	17	1862	79	14.50	12.75	5.18
The building	29.20	1044	74	10.86	8.67	6.74

Table 4.2 : The first natural periods of the building before, after, and during the earthquake.

No	Date	Period (s)		
		Initial Time/ Duration (min)	EW Dir.	NS Dir.
1	July 5, 2019	02:00 / 20	0.87	1.00
2	July 5, 2019	04:00 / 20	0.87	1.00
3	July 15, 2019	04:00 / 20	0.89	1.01
4	July 25, 2019	02:00 / 20	0.88	1.00
5	Aug 5, 2019	04:00 / 20	0.87	1.01
6	Aug 5, 2019 (Denizli Eq.)	11:25 / <1	0.89	1.02
7	Aug 15, 2019	02:00 / 20	0.87	1.00
8	Aug 25, 2019	02:00 / 20	0.87	1.00
9	Sep 5, 2019	03:00 / 20	0.88	1.01
10	Sep 20, 2019	01:20 / 20	0.89	1.03
11	Sep 24, 2019 (Marmara Eq, Mw=4.4)	11:00 / <1	0.91	1.02
12	Sep 26, 2019 (During the Eq.)	11:25 / <1	0.93	1.03
13	Sep 28, 2019	04:00 / 20	0.90	1.01
14	Sep 29, 2019	04:00 / 20	0.90	1.01
15	Oct 5, 2019	04:00 / 20	0.89	1.01
16	Oct 9, 2019	02:00 / 20	0.91	1.01
17	Oct 10, 2019	04:00 / 20	0.91	1.01
18	Oct 20, 2019	02:00 / 20	0.90	1.01
18	Oct 28, 2019	21:00 / 20	0.91	1.01
19	Nov 10, 2019	04:00 / 20	0.90	1.01
20	Nov 20, 2019	02:00 / 20	0.92	1.01
21	Dec 10, 2019	02:00 / 20	0.91	1.01
22	Dec 20, 2019	02:00 / 20	0.90	1.01
23	Jan 10, 2020	02:00 / 20	0.90	1.01
24	Jan 11, 2020 (Manisa Eq.)	16:36 / <1	0.93	1.02
25	Jan 20, 2020	04:00 / 20	0.91	1.01
26	Feb 10, 2020	02:10 / 30	0.91	1.01
27	Feb 20, 2020	02:00 / 20	0.91	1.02
28	Mar 10, 2020	02:00 / 20	0.91	1.02
29	Mar 20, 2020	02:00 / 20	0.92	1.01
30	Apr 10, 2020	02:00 / 20	0.91	1.01
31	Apr 20, 2020	02:00 / 20	0.92	1.02
32	Apr 25, 2020	04:00 / 20	0.92	1.02
33	May 1, 2020	02:00 / 20	0.88	1.01
34	May 2, 2020	02:00 / 20	0.88	1.01
35	May 3, 2020	02:00 / 20	0.88	1.01

Secondly, the first natural periods analyzed by OMA of the building are shown in table 4.2. In the table, a total of 35 analyses are presented, 10 of which are before the earthquake, 24 of which are after the earthquake, and 1 of which are during the earthquake. The conclusion of these analyses are listed below:

- The average of the first natural periods of the building before the earthquake in the EW and NS directions are 0.88 and 1.01 seconds, respectively.
- The first natural period of the building before the earthquake changes from .87 to .91 seconds in the EW direction while it changes from 1.00 to 1.02 seconds for in the NS direction.
- During the earthquake, the predominant periods of the building are 0.93 and 1.03 in the EW and NS directions, respectively.
- The average of the first natural period of the building after the earthquake in the EW and NS direction are 0.90 and 1.01 seconds, respectively.
- The first natural period of the building after the earthquake changes from .87 to .91 seconds in the EW direction while it changes from 1.00 to 1.02 seconds for in the NS direction.

As given in Table 4.3 and Table 4.4, the higher modes of the building in the EW and NS directions are compared to the OMA with model analyses of the FE models of the building.

Table 4.3 : Natural periods of the building and error values in the EW direction.

EW direction	Natural Period (T) and Error Calculation					
	1st analysis		2nd analysis		3rd analysis	
	1st T(s)	Error (%)	2nd T(s)	Error (%)	3rd T(s)	Error (%)
Corrected structural model	1.32	45.05	0.37	37.04	0.19	11.76
Updated structural model	0.80	12.09	0.22	18.15	0.11	32.94
Structural model with only infill walls	1.04	14.29	0.30	11.11	0.16	5.88
Structural model with infill walls and soil-structure interaction	0.98	7.69	0.27	0.00	0.14	17.65
Monitoring result	0.91	-	0.27	-	0.17	-

Table 4.4 : Natural periods of the building and error values in the NS direction.

NS direction	Natural Period (T) and Error Calculation					
	1st analysis		2nd analysis		3rd analysis	
	1st T(s)	Error (%)	2nd T(s)	Error (%)	3rd T(s)	Error (%)
Corrected structural model	1.71	69.31	0.44	51.72	0.21	19.23
Updated Structural model	1.03	1.98	0.27	6.90	0.12	20.00
Structural model with only infill walls	1.24	22.77	0.37	27.59	0.12	20.00
Structural model with infill walls and soil-structure interaction	1.12	10.89	0.30	3.45	0.14	6.67
Monitoring result	1.01	-	0.29	-	0.17	-

The natural periods of the corrected structural FE model with expected concrete strength and load distribution are calculated with around 45% and 70% error for the first period, 37% and 51% error for the second period, and 12% and 19% for the third period in EW and NS direction, respectively. Even though updating the FE model only changing the elastic modulus of the concrete of the building concludes the most lower error in the NS direction for the first period, it does not present the same result in the higher modes in both directions and the first natural period in EW direction. After correcting the model with infill walls and soil-structure interaction, the error compared to monitoring result changes between 0% and 18% for each mode period.

Figures 4.1, 4.2, 4.3, 4.4, 4.5, and 4.6 are mainly provided to investigate the relationship between mode shapes of both system identification and FE models. In the legend of the figures, FE model (infill walls) and FE model (infill+soil) represent the structural model with only infill walls and structural model with infill walls and soil-structure interaction, respectively. Normalized modal displacements are used in the graphs. While the effects of infill walls can be seen for higher modes, the soil-structure interaction directly influences the system behavior for each model between -7F and 0F where the building has connections with soils. Even though, the first and second modes for each model have a quite similar trend, the tendency of the third mode changes because of the nonstructural elements and soil-structure interaction.

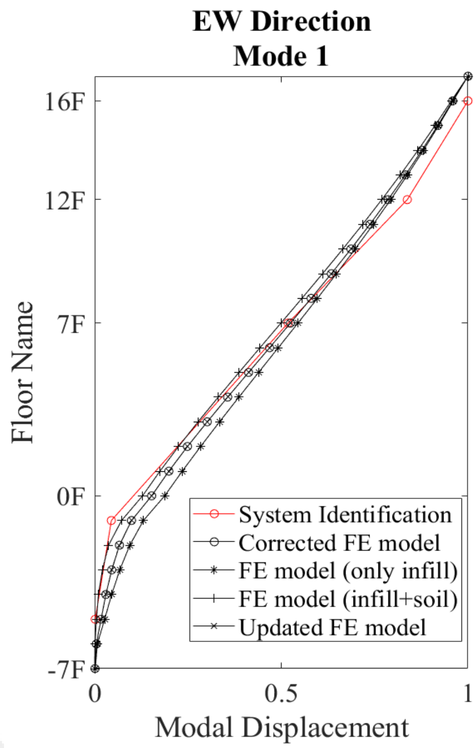

Figure 4.1 : Mode shapes of system identification and each mathematical model for the first mode in the EW direction.

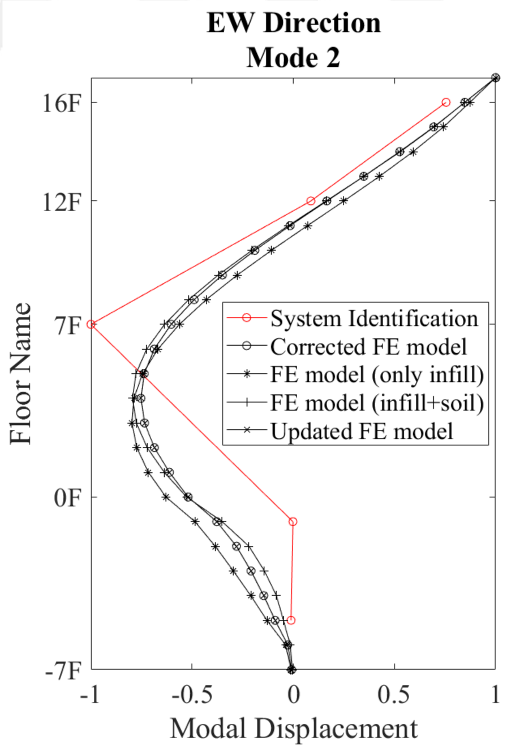

Figure 4.2 : Mode shapes of system identification and each mathematical model for the second mode in the EW direction.

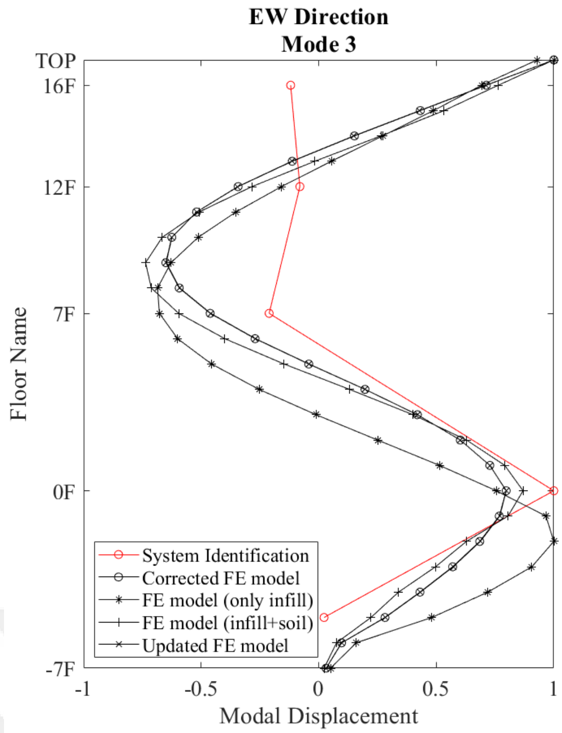

Figure 4.3 : Mode shapes of system identification and each mathematical model for the third mode in the EW direction.

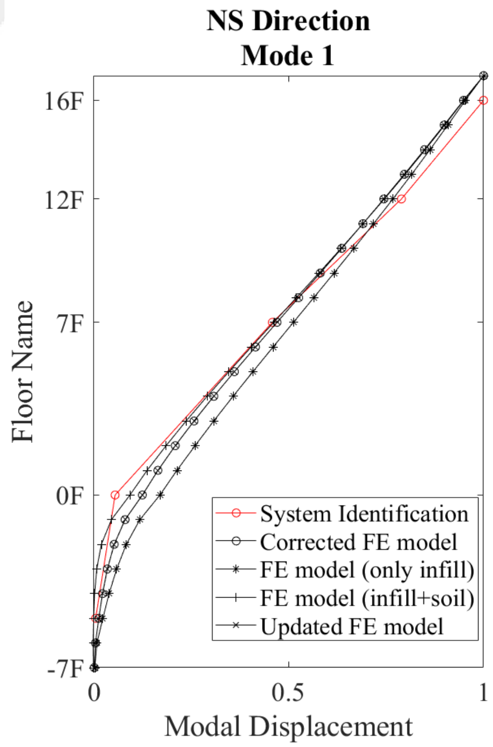

Figure 4.4 : Mode shapes of system identification and each mathematical model for the first mode in the NS direction.

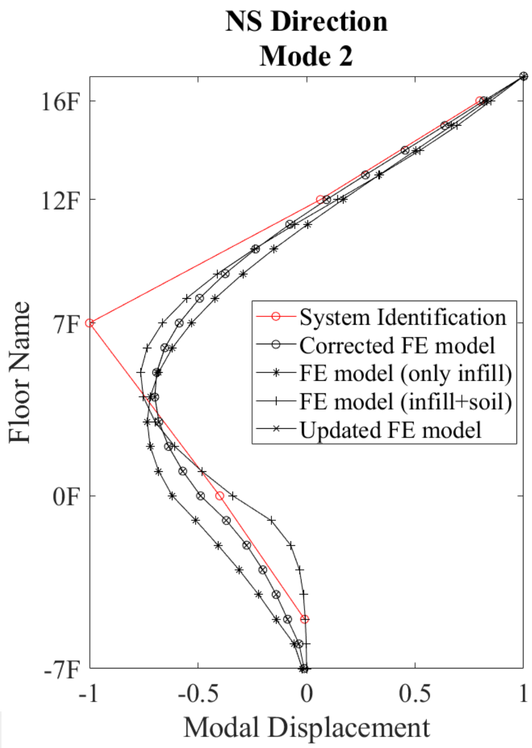

Figure 4.5 : Mode shapes of system identification and each mathematical model for the second mode in the NS direction.

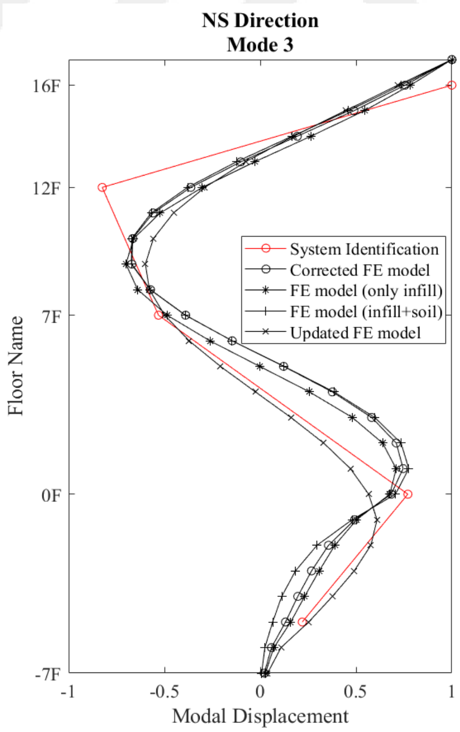

Figure 4.6 : Mode shapes of system identification and each mathematical model for the third mode in the NS direction.

Finally, the comparison of the result of the structural health monitoring of the building during the earthquake with the time linear history analyses of FE models for both calculated and suggested damping ratios can be seen in Table 4.5 and Table 4.6. In the tables, the peak results of acceleration, velocity, and displacement histories of the building on the 16th floor are represented. The error components are calculated according to the results of MATLAB code.

Table 4.5 : The results of the response of the building during the earthquake and error values for EW direction.

EW direction	Damping Ratio (%)	Acc. (Gal)	Error (%)	Vel. (cm/s)	Error (%)	Disp. (cm)	Error (%)
Corrected structural model	1.4	15.40	37.81	-0.94	26.41	0.27	5.38
	2.5	12.64	48.99	-0.84	34.14	0.25	4.22
Updated structural model	1.4	-32.56	31.45	-2.24	75.00	0.28	6.54
	2.5	-28.22	13.93	-1.95	52.58	0.24	7.69
Structural model with only infill walls	1.4	-31.07	25.43	-2.04	59.38	-0.23	11.54
	2.5	-22.42	9.49	-1.52	18.75	-0.20	23.08
Structural model with infill walls and soil-interaction	1.4	-30.00	21.13	-1.69	31.88	-0.25	2.43
	2.5	-20.66	16.58	-1.29	0.55	0.23	11.76
MATLAB Code	1.4	24.76	-	1.28	-	0.26	-

Table 4.6 : The results of the response of the building during the earthquake and error values for NS direction.

NS direction	Damping Ratio (%)	Acc. (Gal)	Error (%)	Vel. (cm/s)	Error (%)	Disp. (cm)	Error (%)
Corrected structural model	0.9	-23.51	31.41	-1.35	56.30	-0.29	30.04
	2.5	-20.64	39.79	-1.31	57.60	0.27	36.11
Updated structural model	0.9	29.65	13.51	-2.30	25.32	-0.39	5.24
	2.5	21.77	36.49	-2.07	32.79	-0.34	19.05
Structural model with only infill walls	0.9	36.38	6.13	-3.13	1.62	-0.43	2.38
	2.5	-26.70	22.11	-2.30	25.32	0.33	21.43
Structural model with infill walls and soil-interaction	0.9	-27.82	18.84	-2.34	24.19	0.41	1.43
	2.5	-26.84	21.70	1.96	36.43	-0.36	14.40
MATLAB Code	0.9	34.26	-	3.03	-	0.42	-

According to Tables 4.5 and 4.6, it is seen that the results obtained for the calculated damping ratio give lover results for almost each of them than the results for the suggested damping ratio. The highest decrease of error for displacement is obtained in the corrected FE model of the building for both directions.

Even though the stiffness of the building rises with including the rigidities of the infill walls and soil-structure interaction to the FE model, it is observed that the displacement also increases in the NS direction. To clarify the reason for that case, the elastic response spectra of the earthquake for %2.5 damping is calculated, given in Figure 4.7 and Figure 4.8 for both directions. In the figures, blue and orange lines respectively demonstrate the periods of the corrected structural model and the FE model with infill walls and soil-structure interaction on the response displacement-period graphs of the earthquake.

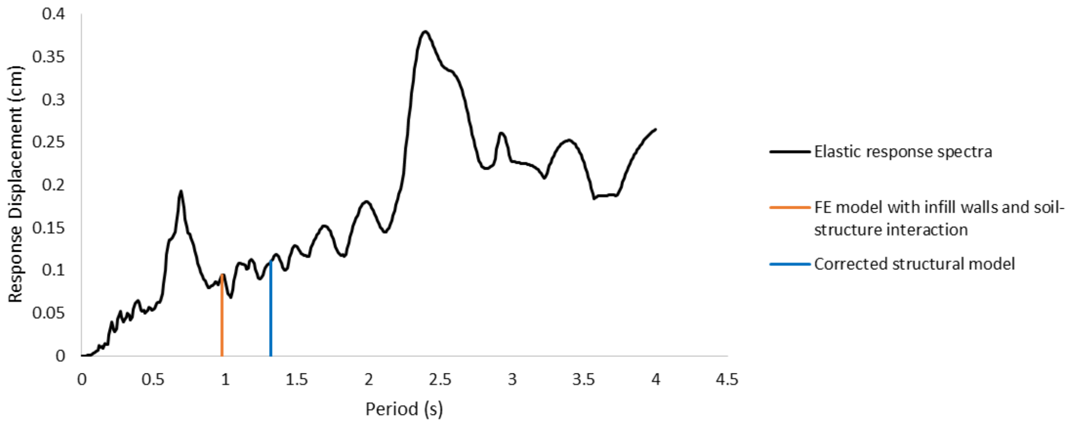

Figure 4.7 : Response displacement-period graph of the earthquake in the EW direction.

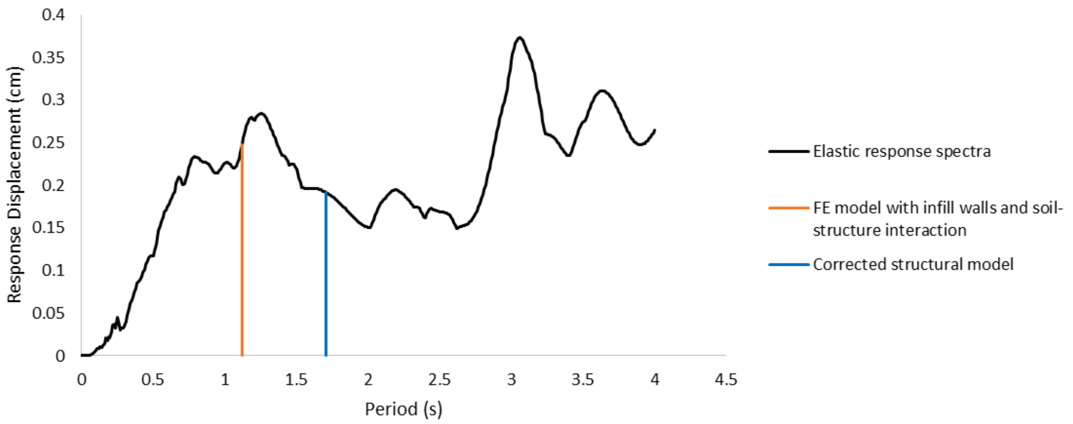

Figure 4.8 : Response displacement-period graph of the earthquake in the NS direction.

According to Figure 4.7, while the period increases between 1 to 2 seconds, the response displacement decreases at the same time in the EW direction. However, one can see the opposite of this trend for the NS direction as shown in Figure 4.8. The fluctuation in the response displacement of the earthquake explains the reason for the alteration of the displacement outcomes for each FE model. Additionally, elastic response spectra of the previous major earthquakes are given in Figure 4.9 to compare to the response of the Marmara earthquake.

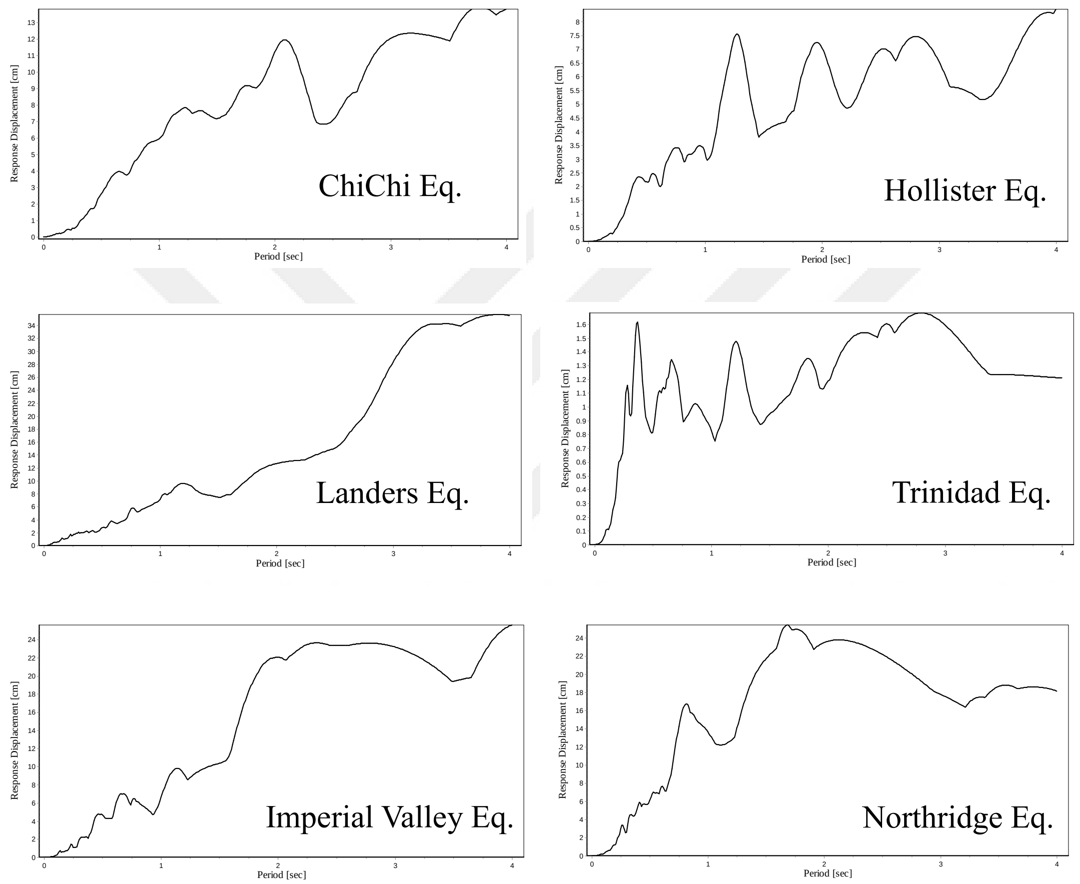

Figure 4.9 : Response displacement-period graph of some major earthquakes.

While the earthquakes on the left-hand side of the Figure demonstrate a similar trend with the earthquake response in the EW direction, the earthquakes on the right-hand side of the Figure have a related fluctuation in the earthquake response in the NS direction.

In addition, the crack detections are carried out in the structural model with infill walls and soil-structure interaction for critical locations of the building. The tensile stress distribution in the concrete of the critical slabs and core walls of the building are investigated. The stress distributions for the EW and NS direction of the critical slab are shown in Figure 4.10. The legend of the distribution with the unit of kN/m^2 is also demonstrated in Figure 4.10.

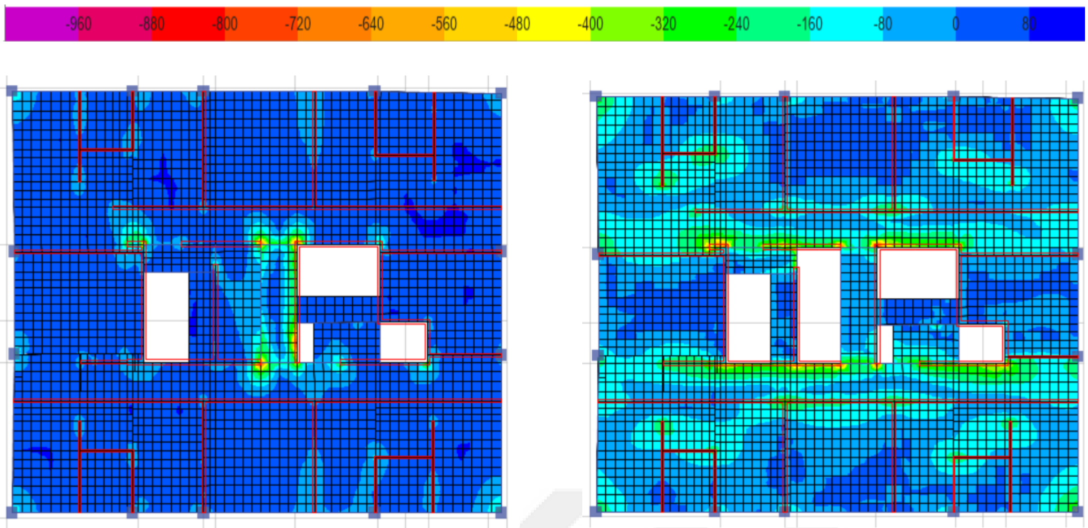

Figure 4.10 : Tensile stress distribution in the concrete of the slab for EW and NS directions from left to right in the figure.

The tensile strength of the concrete is defined as 2200 kN/m^2. The maximum stress in the slab is 890 kN/m^2, which is lower than the tensile strength of the concrete. Therefore, no cracks occur in the slab sections of the building. That also indicates that assigning rigid or semi-rigid diaphragm to the slabs is not needed.

The location of the investigated core walls of the building is marked in Figure 4.11. Besides, the tensile stress distribution in concrete is of the core wall is shown in Figure 4.12 with the legend of the distribution in the unit of MPa. The result of analyzing the maximum tensile stress of concrete on the core walls is 1.32 MPa, which is also lower than the tensile strength of the concrete. Consequently, the result of crack detection in the FE model fits the results of the natural period analyses of ambient vibration, which change slightly before and after the earthquake. As a result, the building has a linear behavior during the earthquake according to experimental and mathematical study.

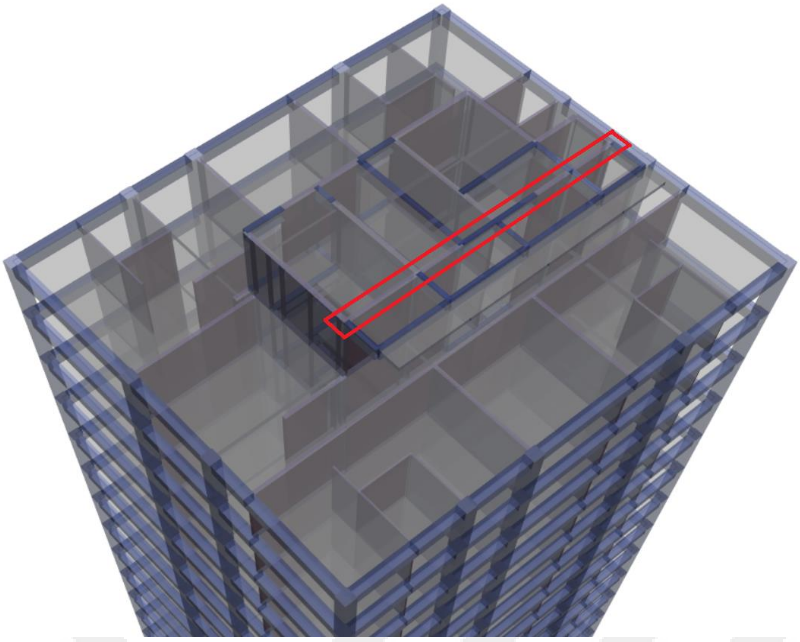

Figure 4.11 : The location of core walls in the zoomed view of the FE model with infill walls and soil-structure interaction.

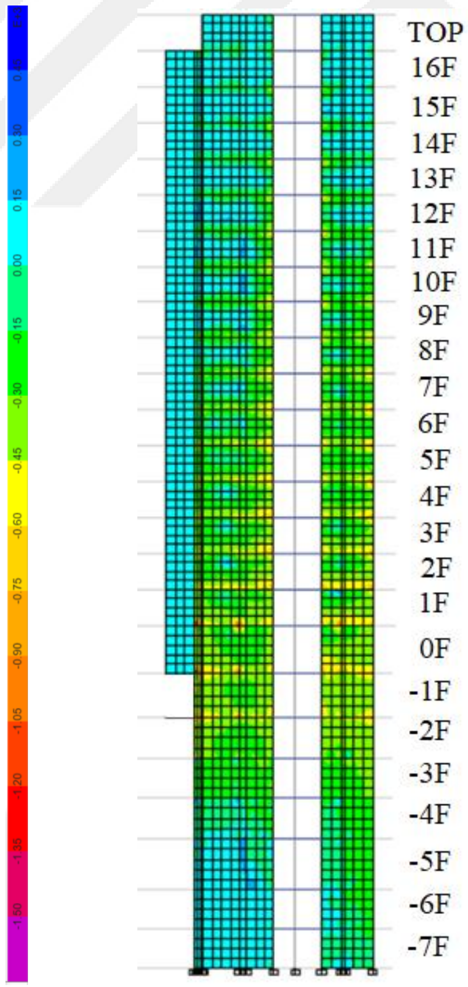

Figure 4.12 : Tensile stress distributions in the concrete of the core walls.

5. CONCLUSION

The main objective of the dissertation is to correct the finite element model of a high-rise building based on the investigation of structural health monitoring of the building. For this purpose, instrumentation, data acquisition, system identification, structural health monitoring of the building, finite element modeling, and procedures of correcting the FE model of the building are covered in the study.

The dissertation is can be divided into three engaging parts:

The first part of the dissertation aimed to investigate the structural health monitoring of the high-rise building. The data acquisition system was installed to make an experimental study on the building. This step is the most important part of the study since it is the initial point and has the potential to affect the whole study. First, accurate types of sensors, receiver, cables, and the locations of the sensors were selected to accurately gather data. After installing the data acquisition system on the building, the different methods are applied to obtain the desired outcome during the system identification process. The selection of the methods is also very important by means of the analyses of the dynamic characterization and behavior of the building. FDD is applied and the first natural periods before an earthquake and the first three periods and mode shapes of the building after the earthquake are obtained with care. In addition to OMA, the building is also investigated during the earthquake with a magnitude of 5.8. The FFT and PSD are applied and the predominant period of the building is identified. According to in-situ measurement, the raw data taken the building on the 16th floor is integrated into velocity and displacement. The raw data is cleaned from the undesired noise components by baseline correction and Butterworth filtering technique for data processing before applying the integration technique. In addition to the conventional approach, WT is also applied to the signal without applying any filtering technique in order to find velocity and displacement time history. The package software program, SeismoSignal, is used to check in order to be sure about the analyses examined during the earthquake.

In the second part of the dissertation, procedures of correcting the FE model of the building based on the system identification was presented. In the FE modeling phase, modal analyses and the linear time history analyses were examined for each mathematical model. For the linear time history analyses, the input taken from the on-site measurement of the building on the -7th floor was used. Additionally, while a damping ratio of the building was is to 2.5% in both directions according to TSDC 2018, it is set 1.4% in the EW direction and 0.9% in the NS direction based on field measurement. The starting point was modeling the building taking loads, reduction factors, and compressive strength of the concrete according to the design phase. Then, the model was updated using altering the compressive strength of the concrete to the expected compressive strength of it. Besides, the live loads with a reduction factor, and the additional wall loads were changed. First, the structural model was updated with respect to these changes. Secondly, the existing infill walls on the structure were modeled on the structural model. Finally, the model was corrected by including both infill walls and soil-structure interaction, which influence the behavior of the building. On the other hand, the model was also updated changing only the elastic modulus of the concrete which is able to give the closest first natural period with the result of system identification of the building in one direction.

The final part of the dissertation presented the comparison of the results of the SHM of the building and each correcting step of the mathematical model. For this aim, the results of system identification were compared with the model analyses of each FE model of the building. Moreover, the response of the building during the earthquake was compared to the results of the time history analyses of the analytical models. In addition to comparison, response displacement of the ınput measured by accelerometer on -7th floor was expressed.

The following results and key points are obtained:

• Fikirtepe, Istanbul region where the building located exposed to the low magnitude of the acceleration during the earthquake because of high shear wave velocity distribution.

• FDD technique is applied to obtain the first, second, and third modes of the natural period of the building and to extract mode shapes of the building.

- The natural period of the building slightly changes before, after, and during the earthquake, which is the indication of linear behavior of the building during the earthquake.
- Predominant response frequency bands are decomposed by the Wavelet Transform method efficiently.
- Instead of using the conventional filtering technique, it is possible to obtain predominant vibration using Wavelet Transform is proposed.
- According to the WT method, displacement decreased by about 15% in the EW direction while it remained at about almost the same in the NS direction.
- The period of the FE model, which considers the design phase, resulted in a 53% error in the EW direction and 81% error in the NS.
- It is needed to increase the elastic modulus of the concrete up to 102,000 MPa to provide the first natural period of the existing building in one direction. It is not realistic to update the FE model only by changing the elastic modulus of the concrete.
- The natural periods of the developed FE model with infill walls and soil-structure interaction are calculated with 8% and 11% error for the first period, 0% and 3.5% error for the second period, and 17.65% and 6.67% for the third period in EW and NS direction, respectively.
- By correcting the model, the error of the displacement decreases to 2.43% in the EW direction and 1.43% in the NS direction.
- Time history analyses give more precise results in terms of calculated damping ratios, which are 1.4% in the EW direction and 0.9% in the NS direction, than 2.5% of the damping ratio defined by the TSDC 2018.
- It is observed that modeling the infill walls as shell elements is effective for ambient vibration and vibration with low magnitude.
- The mode shapes of the corrected FE model of the structure quite match to the system identification results.
- The mode shapes and higher modes of the structure are highly affected by soil-structure interaction.

- Even though the increase of stiffness of the building in NS direction, the displacement increases due to the increase of response displacement of the earthquake from 1 second to 2 seconds.

- Modeling the structure with more precise modal parameters better represents the real behavior of the structure during the earthquakes.

For further studies, the following based on the summarized study above can be suggested;

- Sketching capacity curve of the building using the FEM method and the WT decomposition method,

- Estimating the nonlinear capacity curve for high-rise building using a limited number of sensors, and

- Developing an algorithm to evaluate the health of the structure automatically based on capacity curve estimation.

REFERENCES

[1] **Housner, G., Bergman, L.A., Caughey, T.K., Chassiakos, A.G., Claus, R.O., Masri, S.F., Skelton, R.E., Soong, T., Spencer, B. and Yao, J.T.**, 1997. Structural control: past, present, and future, Journal of engineering mechanics, 123(9), 897–971.

[2] **Worden, K., Farrar, C.R., Manson, G. and Park, G.**, 2007. The fundamental axioms of structural health monitoring, Proceedings of the Royal Society A: Mathematical, Physical and Engineering Sciences, 463(2082), 1639–1664.

[3] **Aktan, A., Catbas, F., Grimmelsman, K. and Tsikos, C.**, 2000. Issues in infrastructure health monitoring for management, Journal of Engineering Mechanics, 126(7), 711–724.

[4] **Abdo, M.A.B.**, 2014. Structural health monitoring: history, applications and future, A review book. Open Science.

[5] **Kusunoki, K. and Teshigawara, M.**, 2004. Development of real-time residual seismic capacity evaluation system–integral method and shaking table test with plain steel frame, 13th world conference on earthquake engineering, CD-Rom, Beijing, China.

[6] **Kusunoki, K., Elgamal, A., Teshigawara, M. and Conte, J.P.**, 2008. Evaluation of structural condition using Wavelet transforms, 14th World Conference on Earthquake Engineering, Beijing, China.

[7] **Kusunoki, K., Tasai, A. and Teshigawara, M.**, 2012. Development of building monitoring system to evaluate residual seismic capacity after an earthquake.

[8] **Kusunoki, K.**, 2016. Damage Evaluation of A Base- Isolated Building With Measured Accelerations During Tohoku Earthquake, the 16th World Conference on Earthquake Engineering, Digital.

[9] **Zhou, Y., Zhou, Y., Yi, W., Chen, T., Tan, D. and Mi, S.**, 2017. Operational modal analysis and rational finite-element model selection for ten high-rise buildings based on on-site ambient vibration measurements, Journal of Performance of Constructed Facilities, 31(5), 04017043.

[10] **Mohammed, M.A., Yu, H., Furtado, A., Barbosa, A.R., Moaveni, B., Varum, H., Rodrigues, H., Vila-Pouca, N. and Wood, R.L.**, 2017. Post-earthquake field measurement-based system identification and finite element modeling of an 18-story masonry-infilled RC building, International Conference on Experimental Vibration Analysis for Civil Engineering Structures, Springer, pp.746–757.

[11] **Rainieri, C., & Fabbrocino, G.**, 2014. Operational modal analysis of civil engineering structures. Springer, New York, 142, 143.

[12] **Valens, C.** 1999. A really friendly guide to wavelets. ed. Clemens Valens.

[13] **Brincker, R., Zhang, L., & Andersen, P.**, 2000. Modal identification from ambient responses using frequency domain decomposition. In Proc. of the 18. International Modal Analysis Conference (IMAC), San Antonio, Texas.

[14] **AFAD** <https://www.afad.gov.tr>, date retrieved 26.09.2019.

[15] **Dorji, J., & Thambiratnam, D. P.**, 2009. Modelling and analysis of infilled frame structures under seismic loads. The open construction and building technology journal, 3(1).

[16] **Celik, O.C.**, 2016. Effect of AAC infill walls on structural system dynamics of a concrete building, Journal of Earthquake Engineering, 20(5), 738–748.

[17] **Venture, N. C. J.** 2012. Soil-structure interaction for building structures. Nist Gcr, 12-917.

[18] **Chopra, A.K.**, 1995. Dynamics of structures theory and applications to earthquake engineering: Prentice Hall international series in civil engineering and engineering mechanics.

[19] **Turkey Building Earthquake Code** 2018, Ankara, Turkey

[20] **ACI Committee 318**, 2008, "Building Code Requirements for Structural Concrete (ACI 318-08) and Commentary", American Concrete Institute, Farmington Hills, MI.

[21] **BS EN 1992-1-1** 2005, "Eurocode 2: Design of Concrete Structures", British Standard Institution, London.

[22] **Turkish Standards Institute**, "TS-500 Building Code Requirements for Structural Concrete", Ankara.

[23] **Kanli, A. I., Tildy, P., Prónay, Z., Pinar, A., & Hermann, L.**, (2006). VS 30 mapping and soil classification for seismic site effect evaluation in Dinar region, SW **Turkey**. Geophysical Journal International, 165(1), 223-235.

CURRICULUM VITAE

Name Surname : Berkay ALDIRMAZ

Place and Date of Birth : Denizli/15.02.1993

E-Mail : berkayald@gmail.com

EDUCATION :

- **B.Sc.** : 2016, Istanbul Technical University, Department of Civil Engineering
- **M.Sc.** : 2020, Istanbul Technical University, Structural Engineering

PROFESSIONAL EXPERIENCE:

- 2019- Present, Scholarship Holder at The Scientific and Technological Research Council of TURKEY (TUBITAK).
- 2017-2019, Research Assistant at Nisantasi University, Istanbul